GIScience & Remote Sensing

ISSN: (Print) (Online) Journal homepage: https://www.tandfonline.com/loi/tgrs20

Towards accurate individual tree parameters estimation in dense forest: optimized coarse-to-fine algorithms for registering UAV and terrestrial LiDAR data

Yuting Zhao, Jungho Im, Zhen zhen & Yinghui Zhao

To cite this article: Yuting Zhao, Jungho Im, Zhen zhen & Yinghui Zhao (2023) Towards accurate individual tree parameters estimation in dense forest: optimized coarse-to-fine algorithms for registering UAV and terrestrial LiDAR data, GIScience & Remote Sensing, 60:1, 2197281, DOI: 10.1080/15481603.2023.2197281

To link to this article: https://doi.org/10.1080/15481603.2023.2197281

© 2023 The Author(s). Published by Informa UK Limited, trading as Taylor & Francis Group.

View supplementary material

Published online: 10 Apr 2023.

Submit your article to this journal

Article views: 456

View related articles

View Crossmark data

Full Terms & Conditions of access and use can be found at
https://www.tandfonline.com/action/journalInformation?journalCode=tgrs20

GISCIENCE & REMOTE SENSING
2023, VOL. 60, NO. 1, 2197281
https://doi.org/10.1080/15481603.2023.2197281

Taylor & Francis
Taylor & Francis Group

OPEN ACCESS Check for updates

Towards accurate individual tree parameters estimation in dense forest: optimized coarse-to-fine algorithms for registering UAV and terrestrial LiDAR data

Yuting Zhao[a], Jungho Im[b], Zhen zhen[a] and Yinghui Zhao[a]

[a]Key Laboratory of Sustainable Forest Ecosystem Management-Ministry of Education, Northeast Forestry University, Harbin, P.R. China; [b]Department of Urban and Environmental Engineering, Ulsan National Institute of Science and Technology, Ulsan, South Korea

ABSTRACT

Accurate quantification of individual tree parameters is vital for precise forest inventory and sustainable forest management. However, in dense forests, terrestrial laser scanning (TLS), which can provide accurate and detailed forest structural measurements, is limited to capturing the complete tree structure due to the lack of upper canopy views, resulting in an underestimation of tree height. Combining TLS with unmanned aerial vehicle laser scanning (ULS) is an effective way to overcome this limitation. Thus, it is vital to register multi-platform Light Detection and Ranging (LiDAR) data for various forestry applications. This study proposed three automated and nearly parameter-free optimized coarse-to-fine algorithms (i.e. FPFH-based optimized ICP (F-OICP), RANSAC-based optimized ICP (R-OICP), and NDT-based optimized ICP (N-OICP)) to accurately register TLS and ULS point data for individual tree crown delineation and parameters (diameter at breast height (DBH) and tree height) estimations in different forest types (i.e. coniferous, mixed broadleaf-coniferous, and broadleaf). Results showed that the proposed optimized algorithms had a good registration performance, with an average RMSE of about 8.3 cm for the transformation error; and obtained stable and high accuracies of individual tree crown delineation (ITCD) (F-score: 0.7), DBH (R^2: 0.9, RMSE <1.85 cm), and tree height (R^2: 0.8, RMSE <0.37 m) estimates for three forest types. F-OICP performed the best in tree height estimation, reducing the RMSE by 48%, 12%, and 12% compared to iterative closest point (ICP), R-OICP, and N-OICP, respectively. Stand type significantly impacted ITCD and individual tree parameter estimations. The ITCD and DBH estimation accuracy of coniferous forests were marginally higher than those of broadleaf forests (F-score: 0.78 vs. 0.78, DBH RMSE: 1.57 vs. 1.74), while those of mixed broadleaf-coniferous forests were the lowest (F-score: 0.71, DBH RMSE: 2.19). The accuracies of tree height estimates in coniferous forests were the highest (R^2: 0.87, RMSE: 0.21 m), followed by mixed broadleaf-coniferous (R^2: 0.84, RMSE: 0.37 m) and broadleaf (R^2: 0.84, RMSE: 0.44 m) forests. This work developed automated, nearly parameter-free, and effective registration algorithms and recommended F-OICP to be the most appropriate for dense forests (i.e. natural secondary forests). The optimized registration algorithms facilitate the ability for the synergistic use of multi-platform LiDAR and offer appealing and promising approaches for future accurate quantification of individual tree parameters, efficient forest inventories, and sustainable forest management.

ARTICLE HISTORY
Received 29 December 2022
Accepted 24 March 2023

KEYWORDS
TLS; ULS; registration; coarse-to-fine; optimized ICP

1. Introduction

Accurately quantifying forest structure is essential for monitoring and understanding how terrestrial ecosystems function and change in response to climate change (Chambers, Asner, and Morton 2007; Le Noë et al. 2021). In particular, accurate measurements of individual tree parameters (e.g. diameter at breast height (DBH) and tree height) are crucial for forest carbon assessment and carbon cycling (Ewald et al. 2018; Zhou et al. 2022). Conventionally, ground-based forest inventory relies on manual tree-by-tree measurements or destructive sampling (Liang and Hyyppä 2013). Manual measurement is extremely tedious and can be difficult to perform in dense or tall trees due to the limited viewing angle. In addition, this measurement method also has many potential error sources, such as requiring individual judgment for each measurement (Madec et al. 2017).

Light Detection and Ranging (LiDAR) data is a non-destructive sensor system and has been widely applied in forest inventory. Initially, its application focused on measuring traditional

CONTACT Zhen Zhen zhzhen@syr.edu; YinghuiZhao yinghuizhao@nefu.edu
Supplemental data for this article can be accessed online at https://doi.org/10.1080/15481603.2023.2197281

© 2023 The Author(s). Published by Informa UK Limited, trading as Taylor & Francis Group.
This is an Open Access article distributed under the terms of the Creative Commons Attribution License (http://creativecommons.org/licenses/by/4.0/), which permits unrestricted use, distribution, and reproduction in any medium, provided the original work is properly cited. The terms on which this article has been published allow the posting of the Accepted Manuscript in a repository by the author(s) or with their consent.

structural metrics used in forestry (e.g. tree height and DBH) but eventually evolved into whole-tree volume and aboveground biomass estimation (Calders et al. 2020). Significantly, the laser beam used in LiDAR can penetrate the forest canopy to acquire the inner information about forest vegetation (Jin et al. 2021). Thus, compared to optical imagery, LiDAR data have incomparable advantages in obtaining forest vertical structural information. The near-surface LiDAR (e.g. terrestrial laser scanning (TLS) and unmanned aerial vehicle laser scanning (ULS)) is a unique and well-established technology that provides convenient methods to obtain three-dimensional (3D) measurements (Zhang, Wan, and Wang 2019; Nunes et al. 2022). Although TLS can provide full data coverage of the tree trunk surface as much as possible through the multi-scan method (Liang, Kankare, and Hyyppä 2016; Chung et al. 2019), the tree crowns derived from TLS data are obscured by other trees due to the bottom-up scanning approach. Therefore, TLS is usually limited to obtaining tree trunk and understory information (Huang, Li, and Gong 2011; Yrttimaa, Saarinen, and Luoma 2019). In addition, researchers have demonstrated that the accuracy of tree attributes, particularly tree height, is relatively inferior when the tree density is between 600 and 1200 stems/ha compared to the low-density forests, for which tree height is easily estimated with high accuracy (RMSE below 20 cm) (Fleck, Mölder, and Jacob 2011; Liang and Hyyppä 2013). Due to the high tree density in dense forests, detecting tree tops from TLS data at a height of about 15–20 m is still challenging (Moskal and Zheng 2012). ULS can conveniently and efficiently provide high-resolution 3D data from upper tree crown (Hyyppä, Holopainen, and Olsson 2012; Brede et al. 2019) but lacks tree trunk information due to the top-down scanning approach (Wallace, Musk, and Lucieer 2014; Balsi et al. 2018). Therefore, researchers employed ULS to assist TLS (Calders, Armston, and Newnham 2014; Wilkes et al. 2018), which can effectively address these limitations, demonstrating significantly improved detection of 3D structure in forests (Kükenbrink, Schneider, and Leiterer 2017; Paris et al. 2017; Morsdorf et al. 2018; Terryn, Calders, and Bartholomeus 2022). However, different densities and scanning angles of multi-platform LiDAR may bring bias in data registration, thereby affecting individual tree parameter estimates (Wang et al. 2022). The point cloud data registration is to find the correspondence between two sets of point clouds with arbitrary coordinate systems and align the two data sets in order to accomplish point cloud fusion (Dai et al. 2019; Zhang et al. 2021). Thus, the point cloud registration algorithm is a key prerequisite for the fusion of multi-platform LiDAR data (Shenkin et al. 2019).

The point cloud registration algorithm usually falls into two categories: coarse and fine registration. Coarse registration is a global alignment method and is usually accomplished by obtaining the geometric features of the point cloud without any assumptions on the initial position (Lu, Wan, and Zhou 2019; Wang and Solomon 2019). Although the common coarse registration algorithms (e.g. 4-points congruent sets (4PCS), scale-invariant feature transform (SIFT)) are generally suitable for engineering applications with regular surfaces, it is challenging to register irregular canopies (Lowe 2004; Aiger, Mitra, and Cohen-Or 2008; Mellado, Aiger, and Mitra 2014). Many current research tends to improve the registration accuracy of ULS and TLS by extracting stable features to reflect the structural information within the canopy: the fast point feature histogram (FPFH) (Rusu et al. 2008) algorithm is an effective and robust feature descriptor that can extract geometric relationships (i.e. the angle difference between the normal vectors of two points and its adjacent points) within a specified range, which has great potential to identify the geometric difference between individual trees; for large-scale dense point clouds (e.g. about 100,000 points); the random sample consensus (RANSAC) algorithm (Raguram, Chum, and Pollefeys 2013) can fit robust models of outlines, calculate the transformation using singular value decomposition, and estimate the feature from point clouds without the influence of noise and outliers; furthermore, the normal distributions transform (NDT) algorithm (Biber and Straßer 2003) achieves coarse registration by calculating normal distribution of each corresponding point and decreasing their distance, which has great efficiency in forests based on point cloud probability density (Magnusson et al. 2009; Hartling, Sagan, and Maimaitijiang 2021). However, it is insufficient to utilize coarse registration to accurately register ULS and

TLS at the individual tree scale and necessary to combine coarse and fine registration algorithm to align canopy details (Paris et al. 2017; Zhang et al. 2021).

Fine registration is dependent on the availability of an initial estimate of the relative position and orientation of the ULS and TLS that is relatively accurate. The iterative closest point (ICP) algorithm is a local registration algorithm that can operate on low-overlapping and large-scale point clouds (Bouaziz, Tagliasacchi, and Pauly 2013). It iteratively matches corresponding points based on a closest distance criterion, and finds the transformation connecting two point clouds (Besl and McKay 1992; Li et al. 2020) and is widely used for point cloud registration in forestry (e.g. Dai et al. 2019; Zhen et al. 2022). However, the ICP algorithm has the limitations of low computational efficiency, restricted convergence domain, and falling into a local optimal solution (Rusu 2010; Li et al. 2020; Zhang, Shao, and Jin 2021). Specifically, the performance of ICP is unstable and inefficient in a dense forest with a massive point cloud data resulting in non-convergence and mismatching (Theiler, Wegner, and Schindler 2015; Paris et al. 2017). K-Dimensional-tree (KD-tree) as an efficient data storage and search algorithm can significantly improve the registration speed of ICP algorithm (Li et al. 2020). The KD-tree algorithm creates a binary tree from the original datasets to modify the data storage structure, gradually reducing the computational complexity (Ren and Wu 2020). However, most of the studies focus on improving the convergence speed and contribute less to improving the stability and robustness of the ICP algorithm using KD-tree (Greenspan and Yurick 2003; Nüchter, Lingemann, and Hertzberg 2007). Currently, it is important to develop an optimized ICP algorithm to accelerate convergence, and more importantly, to increase the stability and robustness of the algorithm for alignment (Li et al. 2016). Therefore, how to extract robust, efficient, and automated point clouds feature descriptors to improve the accuracy of LiDAR data registration to decrease the various errors in individual tree parameters estimation, especially in dense forests, is worth exploring in both fields of forestry and remote sensing.

To overcome the limitations of the traditional registration algorithms (e.g. inefficient calculation, unstable extracted feature descriptors, and local optimal solution) for registering massive point clouds from different LiDAR platforms in dense forests, this study proposed three automated optimized coarse-to-fine algorithms for registering TLS and ULS point cloud data and compared the performances on the estimation of individual tree parameters (i.e. DBH and tree height) in different forest types (i.e. coniferous, mixed broadleaf-coniferous, and broadleaf). The specific objectives were to (1) integrate coverage aware sampling (CAS) into three coarse registration algorithms (i.e. FPFH, RANSAC, and NDT) to efficiently calculate initial positions; (2) utilize KD-tree algorithm to improve ICP algorithm for fine registration and combine it with above three coarse registration algorithms to form three automated optimized coarse-to-fine algorithms, namely FPFH-based optimized ICP (F-OICP), RANSAC-based optimized ICP (R-OICP), and NDT-based optimized ICP (N-OICP); (3) compare the performance of three optimized with traditional ICP algorithm on individual tree parameters estimation for the three forest types; (4) explore the effects of stand type, registration algorithm, and their interaction on individual tree parameters estimation using analysis of variance (ANOVA). This study provided automated optimized coarse-to-fine algorithms to integrate LiDAR point data obtained from different platforms (e.g. TLS and ULS) for accurate and efficient individual tree parameter estimation in dense forests.

2. Materials and methods

2.1. Study area

The study area is located in the Maoershan forest farm (127°29′E–127°44′E, 45°14′N–45°29′N), Shangzhi City, Heilongjiang Province, China (Figure 1). It belongs to the west slope of Zhangguangcailing in the Changbai Mountains. The predominant terrain consists of gentle slopes and low hills, with an average elevation of around 250 m. It is a typical forest ecosystem in northeast China influenced by the temperate continental monsoon climate (Zhen et al. 2022). The forests are currently dominated by natural secondary forests and plantations (Du et al. 2021). The vegetation of the Maoershan region is a component of the Changbai plant flora with an average coverage rate of 95%. The predominant tree species include *Larix olgensis, Pinus koraiensis, Pinus sylvestris, Betula pendula, Juglans mandshurica, Phellodendron amurense* Rupr, and *Ulmus pumila* L var (Liu et al. 2017).

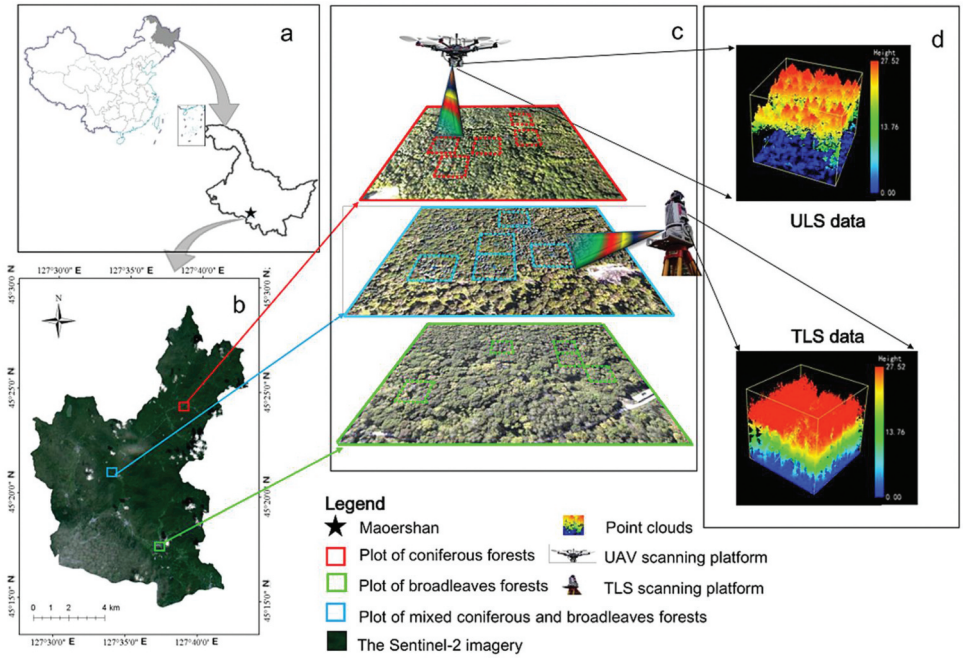

Figure 1. Location of the study area: (a) location of Maoershan in Heilongjiang Province, P.R. China (China Map Examination No. is GS (2019) 1823); (b) Sentinel-2 image (R: Band3; G: Band2; B: Band1) of Maoershan, and the locations of sample plots; (c) distribution of sample plots; and (d) LiDAR point cloud (i.e. TLS and ULS) of one plot. The projection coordinate system for (b) and (c) is WGS 1984 UTM Zone 52N.

2.2. Data collection

2.2.1. LiDAR data

Two types of LiDAR data were used in this study for proposing and evaluating the performance of registration algorithms on individual tree parameter estimation: ULS and TLS. Multiple returns ULS data were collected for 1 km^2 each of coniferous, mixed broadleaf-coniferous, and broadleaf forests in September 2020, August 2021, and July 2022, respectively, using a RIEGL RiCOPTER equipped using the RIEGL mini VUX-SYS system. The flying height was around 90 m above ground level with a line spacing of 30 m, and the UAV flew at a speed of 5 m/s with the overlap of 90%. The average point cloud density of the ULS reached 220–300 points/m^2. The TLS data were acquired for the coniferous, mixed, and broadleaf plots in the summers of 2020, 2021, and 2022, respectively, using a RIEGL VZ-400i terrestrial laser scanner (RIEGL Laser Measurement Systems, Horn, Austria), under the coverage of ULS data. The position accuracy can reach 5 mm at 100 m, and the average point cloud density reaches 190,000–270,000 points/m^2. The essential parameters of the UAV and terrestrial LiDAR data are listed in Table 1. The terrestrial laser scanner was raised around 1.5 m above the ground using a tripod while scanning the sample plots (Yépez-Rincon et al. 2021; Choi and Youngkeun 2022). Due to the high density of trees and shrubs, we chose a dense scanning pattern, setting up 10 ± 3 scanning sites with an approximate distance of 10–

Table 1. Essential parameters of the UAV and terrestrial LiDAR data.

	TLS	ULS
Laser scanning instrument	RIEGL-VZ400i	RIEGL mini VUX-1UAV
Wavelength (nm)	1550	905
Beam divergence (mrad)	0.35	0.5
Effective measurement rate (meas/sec)	420,00–500,000	150
Maximum range (m)	0.5–800	>250
Zenith and azimuth range (◦)	360°	NA
Average point density(points/m^2)	190,000–270,000	220–300

Figure 2. Stand conditions for (a) coniferous; (b) mixed broadleaf-coniferous; and (c) broadleaf forests.

15 m between consecutive scan locations. Each scanning location is connected to the previous and next locations, ensuring that there are scanning sites at the four corner points of the plot. In addition, 5–10 targets with retroreflective surfaces were set up for each plot to ensure thorough scanning and registration. All the scan spots were co-registered using RIEGL RiSCAN PRO software (RIEGL 2020. http://www.riegl.com).

The pre-processing of ULS and TLS data included (1) noise elimination, such as air points, low points, and isolated points; (2) ground and non-ground point classification using an improved progressive triangular irregular network (TIN) densification approach (Zhao et al. 2016); and (3) normalization of point clouds. Additionally, due to the considerable density difference between TLS and ULS point clouds, the TLS data were further resampled using an Octree grid resample with 11 layers (Su, Bethel, and Hu 2016). These pre-processing procedures of LiDAR data were implemented using GreenValley International's LiDAR360 V5.0 (www.lidar360.com).

2.2.2. Reference data. We selected five plots in each stand type based on 2016 Maoershan forest resource inventory data and stand conditions: The coniferous forest plot was a plantation dominated by Larch (*Larix olgensis* Henry) and Korean pine (*Pinus koraiensis* Sieb) with few understory vegetation; the mixed broadleaf-coniferous forest was a natural secondary forest dominated by Korean pine (*Pinus koraiensis* Sieb) and Ash (*Fraxinus mandshurica* Rupr) with complex understory vegetation; the broadleaf forest was a natural secondary forest dominated by Birch (*Betula platyphylla*) and Elm (*Ulmus pumila*) with abundant understory vegetation. The plots from the same stand type have similar species composition, development stages, and vertical structure. To evaluate the performances of registration algorithms of on individual tree parameter estimation in a dense forest, the parameters of all 1306 trees within the 15 sample plots (30×30 m) were collected in the summers of 2020–2022, including DBH (cm), tree height (m), and tree location. The tree height and DBH were measured using the Vertex IV ultrasonic instrument system (Haglofs, Sweden) and a perimeter ruler, respectively, with a starting diameter of 5 cm. The geographic coordinates of each tree and the four corners of the plot were positioned using the Real-time kinematic positioning (RTK) Global Navigation Satellite System (GNSS) (UniStrong G10A, Beijing, China) receiver with a less than 5 cm geographical error (Xu et al. 2020). Due to the weak signal under forest canopy, we ensured the accuracy of the coordinates as follows: (1) the measuring rod on the RTK instrument is set as high as possible, above 2 m; (2) we lasted the measuring time for the trees that are not easy to located, and the average time for RTK-based static control measurement is 10 min; (3) for the trees without signals for a long time, field triangulation/trilateration measurement was conducted according to the accurately positioned trees. The study area is a typical temperate natural secondary forest, with dense and tall canopies and an average stand density of 910 stems/ha. The average stand density of coniferous, mixed broadleaf-coniferous forest, and broadleaf forests are 790, 1160, 760 stems/ha, respectively. All plots are dense forests, and the stand conditions of three forest types (i.e. coniferous, mixed broadleaf-coniferous, and broadleaf) are shown in Figure 2. The mixed broadleaf-coniferous and broadleaf

Table 2. Description statistics for individual tree parameters of all the 15 plots.

Type	Plot	N	Stem density (stems/ha)	DBH (cm)					Tree height (m)				
				Min	Max	Mean	Median	Std	Min	Max	Mean	Median	Std
Coniferous	C-1	41	440	5.7	38.4	23.3	26.8	10.7	5.5	26.3	19.5	24.0	7.9
	C-2	57	630	5.6	42.3	18.4	9.4	13.1	5.1	26.3	15.0	11.3	8.3
	C-3	71	770	6.0	40.8	17.7	11	10.1	5.0	25.9	15.9	11.8	7.9
	C-4	84	930	5.1	33.4	19.2	22	8.1	5.2	25.6	17.9	20.2	6.4
	C-5	104	1200	6.4	33.6	18.1	17.2	6.6	7.2	23.6	18.7	19.6	4.1
	Mean	-	**790**	**5.8**	**37.7**	**19.3**	**17.3**	**9.7**	**5.6**	**25.5**	**17.4**	**17.4**	**6.9**
Mixed	M-1	109	900	5.6	40.5	14.8	12.9	7.2	4.5	23.7	12.6	11.4	4.2
	M-2	116	1000	5.5	48.6	14.8	13.9	7.1	4.3	20.5	12.7	11.7	3.8
	M-3	115	1100	5.4	37.7	15.8	14.4	6.5	5.3	24.2	13.0	13.1	3.9
	M-4	119	1300	6.0	30.9	16.0	15.2	5.8	4.6	23.7	12.1	11.7	3.7
	M-5	145	1500	5.1	30.9	14.8	14.3	5.7	4.5	21.2	12.7	12.3	3.8
	Mean	-	**1160**	**5.5**	**37.7**	**15.2**	**14.1**	**6.5**	**4.6**	**22.7**	**12.6**	**12.0**	**3.9**
Broadleaf	B-1	59	660	6.0	42.3	17.3	16.8	7.7	5.2	24.9	15.6	16.0	5.5
	B-2	60	660	7.9	56.5	21.3	16.5	11.1	8.2	28.1	19.2	18.5	5.6
	B-3	69	770	6.9	39.5	20.9	21.7	8.7	7.1	28.4	18.3	19.1	6.3
	B-4	71	770	7.0	49.2	16.8	14.1	7.9	6.8	29.0	16.7	17.1	4.7
	B-5	86	940	7.0	35.9	16.3	15.5	6.3	6.8	28.5	17.5	18.7	5.1
	Mean	-	**760**	**7.0**	**44.6**	**18.5**	**16.9**	**8.3**	**6.8**	**27.8**	**17.5**	**17.9**	**5.4**

Note: Coniferous represents coniferous forests; mixed represents mixed broadleaf-coniferous forests; broadleaf represents broadleaf forests. N is the number of trees in each plot. Std is the abbreviation of standard deviation.

plots have a complex vertical vegetation structure: shrubs are distributed in clusters and affect the visibility of the tree stems; the upper forest canopy has a huge number of cross-overlapping canopies. The descriptive statistics of individual tree parameters of the 1306 trees are listed in Table 2.

2.3 Methods

We proposed three automated optimized coarse-to-fine algorithms for registering terrestrial and ULS point data to accurately characterize the three-dimensional information of different forests and then evaluated their performances based on individual tree parameter estimation. Four steps were designed in this study (see Figure 3): (1) coarse registration, including utilizing the CAS algorithm to down-sampling TLS and ULS data, registering the down-sampled data using three coarse algorithms (i.e. FPFH, RANSAC, and NDT) separately, and determining the initial positions of the cloud points; (2) fine registration, including utilizing the KD-tree algorithm to accelerate the ICP, registering the initialized positions using the optimized ICP and traditional ICP. The three optimized coarse-to-fine registration algorithms were constructed based on FPFH, RANSAC, and NDT; (3) individual tree parameter estimation, including detecting individual tree crowns and estimating tree height and DBH using the fused LiDAR data based on the three optimized algorithms and traditional ICP; (4) accuracy assessment and ANOVA analysis, including quantifying the transformation errors of registering UAV and terrestrial LiDAR, evaluating the accuracies of individual tree parameter estimates, and conducting a two-way ANOVA to investigate the effect of stand type, registration algorithm, and their interaction on the estimates of individual tree parameters.

2.3.1. Coarse registration

2.3.1.1. Down-sampling LiDAR data

Due to the irregularity of the point cloud data and the significant differences in magnitudes between the TLS and ULS point clouds, the original LiDAR data cannot be directly aligned using coarse registration algorithms. In this study, the CAS (Xu et al. 2020) algorithm was used to down-sample the respective clouds before registering the TLS and ULS data, decreasing the number of redundant points (Terryn, Calders, and Bartholomeus 2022) and improving the stability of coarse registration algorithms. The voxel grid size was chosen based on the beam divergence, and range of the laser scanners and the UAV-LiDAR and TLS data were traversed with voxel sizes of 0.02 and 0.1 m, respectively (Kükenbrink, Schneider, and Leiterer 2017). Subsequently, the points within the voxel were filtered based on the spatial coverage of the points such that they can cover the most occupied space. Down-sampling was stopped when all voxels had been traversed. Since CAS focuses on the

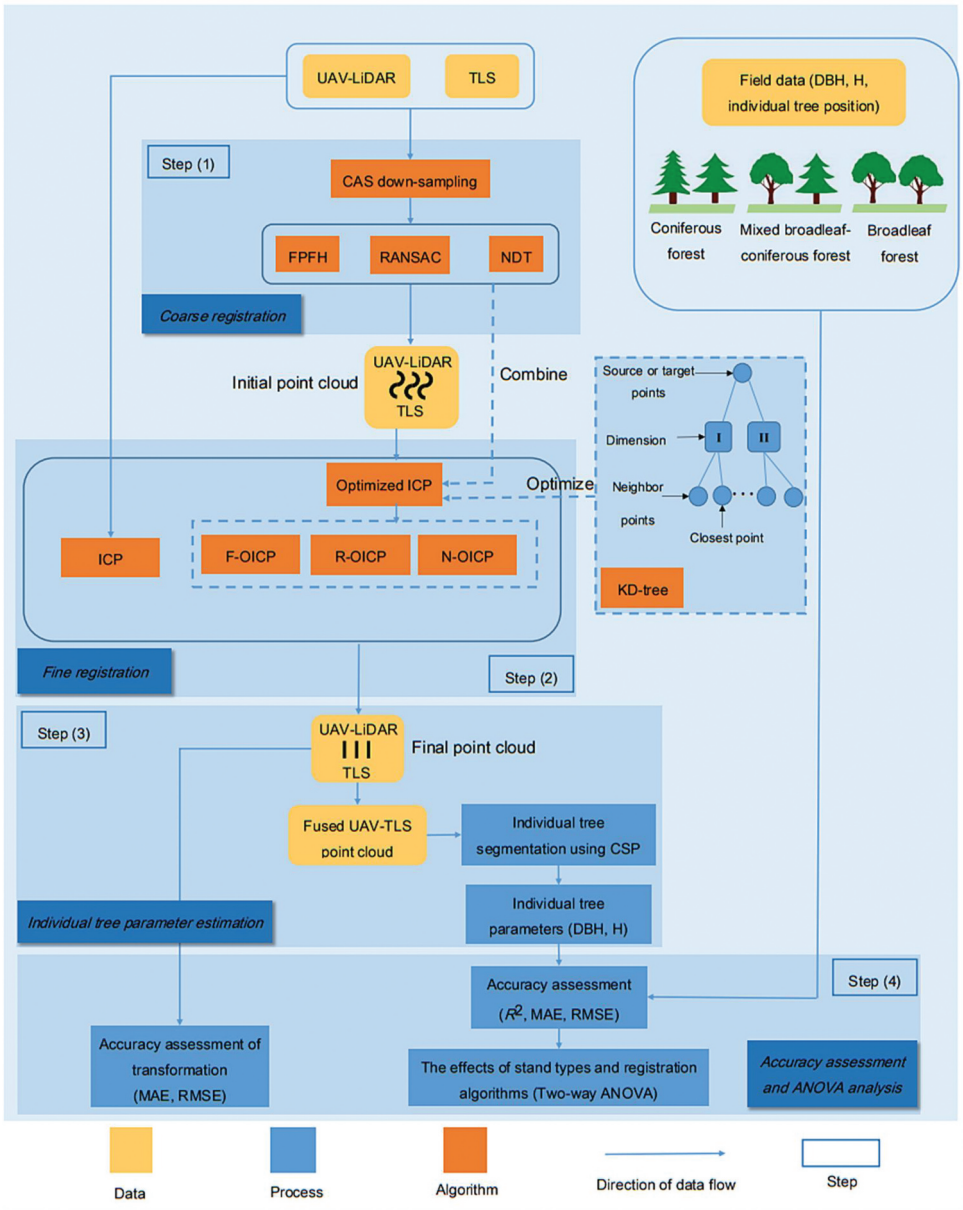

Figure 3. Flowchart of automated registration based on TLS and ULS and performance assessment using the optimized coarse-to-fine algorithm for coniferous, mixed broadleaf-coniferous, and broadleaf forests.

spatial distribution of the points rather than the absolute density, it cannot lose essential features (e.g. normal vector, angle, and keypoint) (Pyörälä, Saarinen, and Kankare 2019).

2.3.1.2. Coarse registration using FPFH

In the coarse registration, three algorithms (i.e. FPFH, RANSAC, and NDT) were utilized to determine the initial point position of the ULS data. The FPFH algorithm, inherited from the Point Feature Histogram (PFH) (Rusu et al. 2008), was designed to generate a robust and stable feature description (Rusu, Blodow, and Beetz 2009). It calculates the geometrical relations between the query point p_i and its k-neighbor points, which incorporates the estimated surface normal of the p_i and the angle difference between the normal vectors and the line connecting the neighbors of p_i and q_j (Wang et al. 2022). These geometric features of the inquiry point (p_i) and its k-neighbors were aggregated to generate the simplified Point Feature Histogram (SPFH) as the feature descriptors. In general, the histogram of feature is normally

distributed and a unique signature of each surface (i.e. the surface perpendicularly intersected the normal vector at point p_i) (Dong, Liang, and Yang 2020). Finally, the FPFH of the point p_i was determined by calculating the SPFH of the k-neighbor by the weight ω_k (Rusu, Blodow, and Beetz 2009) as follows:

$$FPFH_{pi} = SPFH_{pi} + \frac{1}{K}\sum_{i=1}^{K}\frac{1}{\omega_k}\cdot SPFH_{pk} \quad (1)$$

where weight ω_k is the distance between p_i and its k-neighbors. The aim of FPFH is to estimate an optimal rigid transformation of TLS and ULS point clouds.

2.3.1.3. Coarse registration using RANSAC

RANSAC is used to build robust models, remove outliers, and compute transformations using singular value decomposition (Raguram, Chum, and Pollefeys 2013). The first step is to sample a subset of points from the same location of both ULS and TLS data as the local area's centroid and the second step is to locate neighborhood points to build a regional subset called the consensus set (Chum, Matas, and Kittler 2003). Simultaneously, the RANSAC attempts to maximize the cardinality of this set by efficiently exploring the full space of the point cloud (Fischler and Bolles 1987). The third step is to match the consensus subset of the two LiDAR data using the translation and rotation matrices, which can transform the source point (i.e. ULS) to the target point (i.e. TLS).

2.3.1.4. Coarse registration using NDT

This coarse registration aims to minimize the distance of the two NDT models established by the source and target points. The NDT is a model used to describe the spatial distribution characteristics of point clouds using a set of Gaussian probability distributions (Magnusson et al. 2009). First, the probability density functions (PDFs) of two-point clouds data were computed based on the mean and covariance; second, the NDT model was established by the two PDFs of the source and target points; finally, a set of spatial mapping parameters by concatenating the NDT of the source and target points were generated and used to register all of the source and target points. The details of this NDT algorithm were described in Magnusson's (2009).

2.3.2. Fine registration

2.3.2.1. ICP algorithm

After coarse registration of ULS and TLS, fine registration was conducted by traditional ICP (Santamaría, Cordón, and Damas 2011) and three optimized ICP algorithms based on three coarse registration algorithms (i.e. FPFH, RANSAC, and NDT). The ICP algorithm constructs a rigid transformation by matching the query point p_i (the point from ULS) and the corresponding point q_j (the point from TLS) and registers two datasets (i.e. ULS and TLS) accurately through iteration. The process of searching and transforming is repeated until convergence is achieved (Rusu et al. 2008).

2.3.2.2. Optimized ICP algorithm

Although ICP can register the source and target points at a local scale by iteratively minimizing the point-to-point distance when dealing with massive amounts of points, the alignment can easily fall into local minima and the computational complexity is extremely high. To overcome these limitations, the KD-tree algorithm was utilized to optimize ICP and increase the efficiency and accuracy of registration. The KD-tree is capable of effectively managing and organizing massive amounts of information data (Zhang 2016). To enhance the stability of the optimized algorithm, we added two loop structures in the optimized ICP algorithm. Figure 4 shows the detailed scheme of the optimized algorithm that contains inner and outer loops.

The outer loop: (1) Construction of KD-tree. KD-tree was utilized to reconfigure the storage space of the source and target points for improving the computation efficiency. Based on the spatial distribution of the points, the point clouds were separated into different dimensions. When the point clouds are in the same dimension, they are divided into different nodes (see the KD-tree in Figure 3).

(2) Calculation of the minimal distance between the source and target points based on the KD-tree structure. The inner loop was designed by the following steps:

- Step 1: Calculate the distance between the query point p_i and each dimension and search for the dimensional region that is nearest to the query point of the source point data (i.e. ULS).
- Step 2: Calculate the distance between the query point p_i and each node of the target point data (i.e. TLS) in the nearest dimensional region and

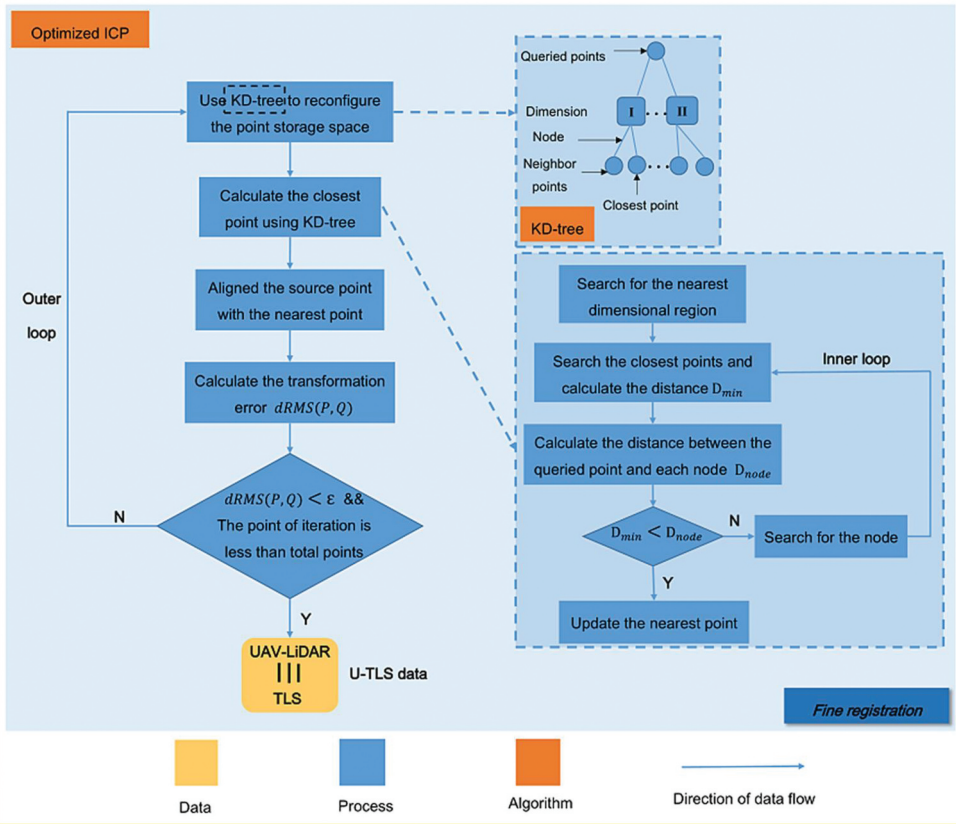

Figure 4. Procedures of the optimized ICP algorithm. The KD-tree was utilized to calculate the nearest point and final point location; the inner loop determined the corresponding point, while the outer loop determined the final point cloud location.

mark the closest point as the original corresponding point (i.e. a point in the TLS data). The minimum distance between a query point (a point in ULS data) and the corresponding point (a point in TLS data) was recorded as $D_{\min}$.

- Step 3: Calculate the distances between the query point and all the nodes in the other dimensions (the minimum distance was recorded as D_{node}) and replace $D_{\min}$ with D_{node} if $D_{node}<D_{\min}$.
- Step 4: Update and determine the closest point by repeating steps 2 and 3.
  1. Align the query point p_i with the closest point (i.e. corresponding point) in TLS data obtained in the previous steps.
  2. Calculation of the transformation error $dRMS(P,Q)$ between the transformed source point and target point. If the $dRMS(P,Q)$ is less than a threshold ε and the number of transformed source points is less than the total number of points, the algorithm converges (or stops); otherwise, the next iteration continues.

$$dRMS(P,Q) = \sqrt{\frac{1}{n}\sum_{i,j=1}^{n}(\| p_i - q_j \|)^2} < \varepsilon \quad (1 \le j \le m)$$

where p_i is the source point (i.e., ULS), q_j is the target point (i.e., TLS), ε is the threshold for the minimum distance between p_i and q_j , and n and m are the numbers of source point and target point, respectively. The "||" represents the Euclidean distance between the source point and the target point. After coarse and fine registration, the ULS and TLS data were fused and defined as U-TLS data.

All experiments were implemented on a standard computer with an Inter(R) Core (TM) i7-12700k CPU @3.0 GHz GPU and 32GB RAM. We implemented all the coarse-to-fine algorithms in C++ with the open-source Point Cloud Library (PCL) (https://pointclouds.org). We integrated a timing system into the code and recorded the running time of the registration algorithm to evaluate the performance of all the algorithms

(LiDAR360 software records the runtime of traditional ICP).

2.3.3. Estimation of individual tree parameters

Based on the U-TLS data, the comparative shortest path (CSP) (Tao et al. 2015) segmentation algorithm was applied to delineate individual trees, and the individual tree parameters (i.e. DBH and tree height) were estimated. The CSP algorithm is a bottom-up region-growing approach designed to segment individual tree crown of TLS-based data (Tao et al. 2015). Since the CSP algorithm fully takes advantage of ecological basis and metabolic ecology theory as guidelines, it can provide a high accuracy of individual crown segmentation in natural secondary forests with a large number of crown intersection and irregular crown shape (West, Brown, and Enquist 1999; Bentley et al. 2013). To improve the segmentation accuracy of the CSP algorithm, we constrained the parameters of the CSP algorithm based on the field data: The minimum DBH and tree height were set to be the smallest DBH and tree height in each plot. These parameters minimized the influence of small trees on ITC segmentation. The DBH was determined by utilizing the non-linear least-squares method to fit a circle for the point cloud between 1.2 and 1.4 m above ground level (Prendes et al. 2021). The highest point within each tree crown was treated as the tree height.

2.3.4. Accuracy assessment

2.3.4.1 Accuracy assessment of registration algorithms

The transformation usually falls into two categories: rigid or non-rigid. The proposed optimized algorithm to register LiDAR point clouds can be solved with a rigid transformation. The transformation error between the corresponding points from registered ULS and TLS data was calculated to quantitatively evaluate the performance of three optimized coarse-to-fine algorithms. Since the distance between corresponding points should be zero for a flawless rigid registration (Zhang et al. 2021), the transformation error of source point and target point can be expressed as the Euclidean distance between corresponding points and was divided into vertical and horizontal directions (Li et al. 2020; Zhang, Shao, and Jin 2021). In this study, the Root Mean Squared Error (RMSE) and Mean Absolute Error (MAE) were applied to evaluate the accuracy of four registration algorithms (i.e. ICP, F-OICP, R-OICP, and N-OICP) as follows:

$$MAE = \frac{1}{n}\sum_{i=1}^{n}\left|x_i - x_i^{'}\right| \tag{3}$$

$$RMSE = \sqrt{\frac{1}{n}\sum_{i=1}^{n}\left(x_i - x_i^{'}\right)^2} \tag{4}$$

Where x_i represents the distance between corresponding points in the vertical or horizontal directions, $x_i^{'}$ represents the distance of truth transformation, and n is the numbers of corresponding points.

2.3.4.2 Accuracy assessment of individual tree crown delineation (ITCD)

The accuracy assessment of ITCD was based on 1:1 matched trees, which were defined by the following three-step procedure: (1) identify all detected trees within a 3 m buffer of each reference tree; (2) determine the detected tree that has the smallest differences in DBH and tree height compared to the reference tree; and (3) remove outliers with absolute values of external studentized residuals greater than three. Three common metrics were applied to evaluate the performance of the CSP algorithm: recall (r), precision (p), and F-score (Jing et al. 2012; Shen and Cao 2017; Yang et al. 2019).

$$r = \frac{TP}{TP + FN} \tag{5}$$

$$p = \frac{TP}{TP + FP} \tag{6}$$

$$F - score = 2 \times \frac{p \times r}{p + r} \tag{7}$$

where TP represents true positive, indicating that a tree was accurately detected, that is, 1:1 matched trees; FN represents false negative, indicating that no tree is detected; and FP represents false positive, indicating that a non-existent tree is detected. The r represents the ratio of true positives to all ground reference trees, while the p represents the ratio of true positives to all detected trees. The F-score considers both omission and commission. TP, FP, and FN

indicate correct segmentation, over-segmentation, and under-segmentation, respectively (Li et al. 2012).

2.3.4.3 Accuracy assessment of individual tree parameters estimations

In this study, the coefficient of determination (R^2) of the regression between estimated and measured parameters and the RMSE and MAE of estimated parameters were used to evaluate the accuracy of individual tree parameters estimation based on 1:1 matched trees (Fang et al. 2016; Zhen et al. 2022).

2.3.5 Investigation of the effects of stand type and registration algorithm

ANOVA is a statistical approach for analyzing the variance of means of ensemble members indicating the variation caused by one or more factors from a specific source alteration (Li, Xu, and Wu 2022). A two-way ANOVA was conducted to investigate the effects of the different registration algorithms (i.e. ICP, F-OICP, R-OICP, and N-OICP) and forest stand types (i.e. coniferous, mixed broadleaf-coniferous, and broadleaf forests) and their interaction on individual tree parameter estimations (Almeida et al. 2019). This study also applied the Tukey's Honest Significant Difference (HSD) test to examine which algorithm's or stand type's mean differed from the others (Gara et al. 2019).

3. Results

3.1. Evaluation of optimized registration algorithms

3.1.1. Visual evaluation

Figure 5 illustrates the visual evaluation of three optimized registration algorithms (i.e. F-OICP, R-OICP, and N-OICP) for three forest stand types (i.e. coniferous, mixed broadleaf-coniferous, and broadleaf forests). The three algorithms showed consistent and excellent registration performance, including the global and detailed registrations (i.e. slices **I, II**, and **III**). Since TLS has a full tree trunk layer point representation, the tree trunk cross-sections can be fitted to a complete circle by all algorithms (slice **I**). However, slices **II** and **III** presented clear differences among the three algorithms: the F-OICP algorithm describes more details (e.g. branches) than R-OICP and N-OICP (see slice **II**); furthermore, the ULS crown registered using F-OICP was closer to the TLS crown's central axis than those registered using the other two algorithms (see slice **III**).

For different stand types, coniferous forests obtained the most outstanding and stable registration results compared to mixed broadleaf-coniferous and broadleaf forests (Figure 5(a)). It is worth noting that there is almost no horizontal offset at the highest point of the canopy of coniferous forest. However, in mixed broadleaf-coniferous and broadleaf forests, even the best-performing F-OICP algorithm generated a slight misalignment at the crown's highest points. This was because broadleaf trees were prone to falling into a local minimum and sliding along flat surfaces due to the irregular crown morphology and leaf shape, resulting in misalignment of the highest point (Terryn, Calders, and Bartholomeus 2022). Visually, we can preliminarily consider that the three optimized algorithms obtained excellent registration performance, especially in the upper canopy.

3.1.2. Quantitative evaluation

To quantify the performance of the three optimized coarse-to-fine algorithms, the transformation error between registered point data was evaluated in the vertical and horizontal directions. From Table 3, we found that all errors (i.e. MAE or RMSE) of the three optimized algorithms in the horizontal and vertical directions were less than 10 cm, with smaller errors in the vertical direction. F-OICP provided better accuracy than R-OICP and N-OICP in both directions for all stand types (horizontal: approximately 1.14 cm lower for MAE and 1.35 cm lower for RMSE; vertical: approximately 1.26 cm lower for MAE and 1.38 cm lower for RMSE). The performances of the optimized algorithms are consistent with Figure 5.

For different stand types, coniferous forest obtained the highest transformation accuracy, followed by mixed broadleaf-coniferous and broadleaf forests. This was because coniferous forests have a more regular crown profile and leaf morphology than broadleaf forests, making them more susceptible to extracting stable features (e.g. the normal and angle of leaf). For the different stands with similar stem density (C-4: 930 stems/ha; M-1: 900 stems/ha; B-5: 940 stems/ha) (Supplementary table S1), the

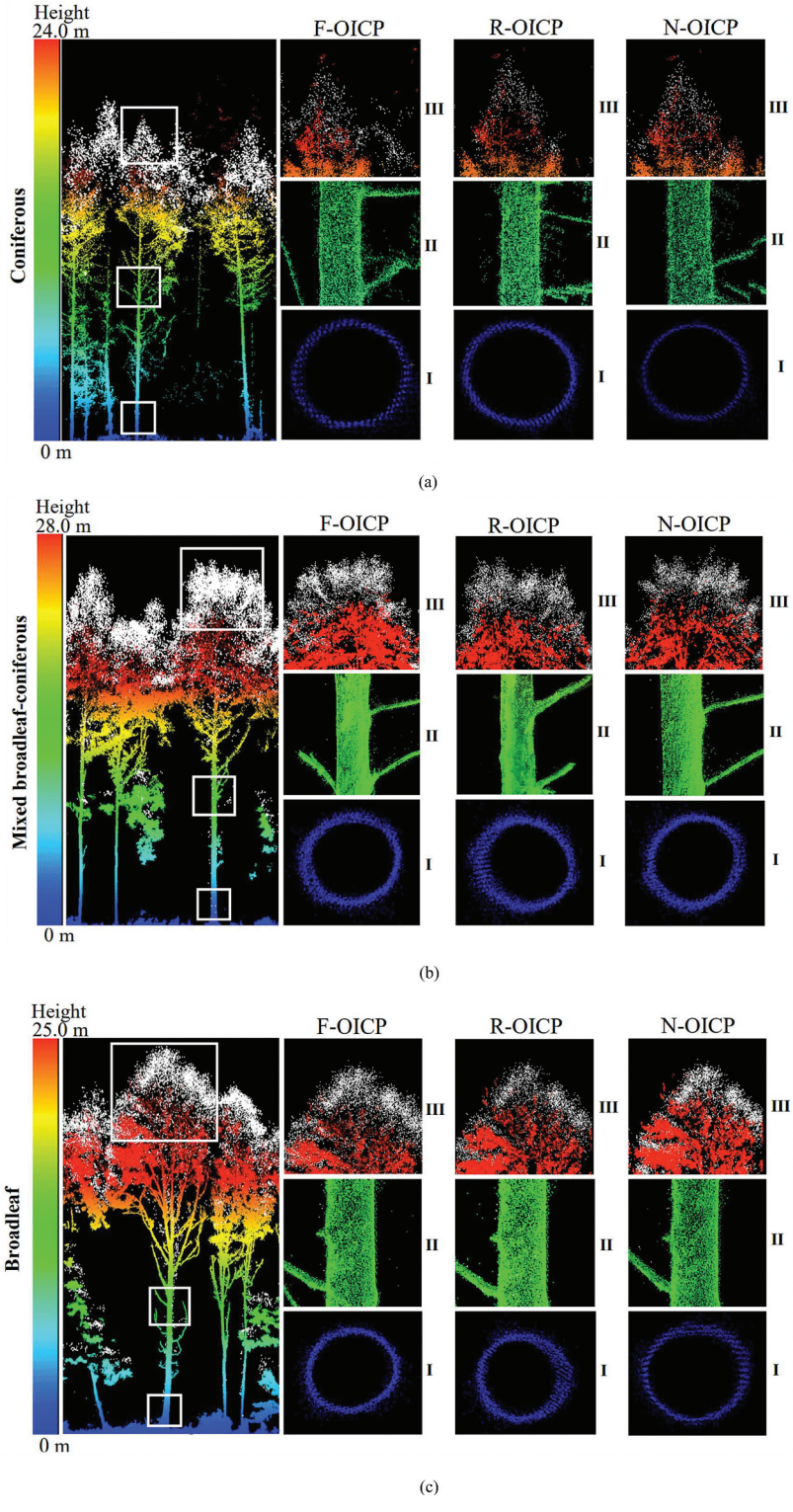

Figure 5. Visual evaluation of the optimized coarse-to-fine algorithms (i.e. F-OICP, R-OICP, N-OICP) for (a) coniferous, (b) mixed broadleaf-coniferous, and (c) broadleaf forests, taking C-5, M-1, and B-2 plot as examples. The white points represent the registered ULS data and the color-rendered points represent the TLS data. Slices I, II, and III represent the sections 1.3 m (DBH) above the ground, tree trunk, and tree crowns, respectively.

Table 3. Accuracy assessment of transformation in horizontal and vertical directions.

Stand type	Stem density (stems/ha)	Statistics	F-OICP		R-OICP		N-OICP	
			MAE (cm)	RMSE (cm)	MAE (cm)	RMSE (cm)	MAE (cm)	RMSE (cm)
Coniferous	790	Mean	3.30/2.56*	4.29/3.38*	4.93/3.19*	6.02/4.31*	5.02/4.00*	6.55/6.78*
		Std	1.94/1.41*	2.43/1.72*	1.45/1.09*	1.69/1.41*	0.87/1.75*	1.01/2.53*
Mixed	1200	Mean	6.59/5.16*	7.58/6.34*	6.96/5.64*	8.04/6.84*	6.70/5.73*	7.86/6.93*
		Std	1.21/1.14*	1.01/1.15*	1.01/1.44*	1.00/1.39*	1.06/1.24*	0.99/1.24*
Broadleaf	760	Mean	9.72/8.40*	13.22/12.37*	11.49/10.86*	15.04/14.21*	10.95/10.34*	14.75/13.42*
		Std	1.22/1.01*	1.51/1.41*	0.89/0.94*	1.13/1.42*	1.13/0.97*	1.06/1.39*
Mean	-	-	**6.54/5.37***	**8.36/7.37***	**7.79/6.56***	**9.70/8.45***	**7.56/6.69***	**9.72/9.04***
Std	-	-	**3.05/2.71***	**4.14/4.10***	**3.03/3.49***	**4.18/4.55***	**2.75/3.05***	**3.84/3.61***

Note: "*" represents the transformation error in the vertical direction. F-OICP, R-OICP, N-OICP represent FPFH-, RANSAC-, NDT- optimized ICP algorithms, respectively. Std represent the standard deviation of the accuracy indices for all the plots.

RMSE of plot M-1 was approximately four times of that of plot C-4 (8.65 vs. 1.92 cm) using F-OICP, while the RMSE of plot B-5 was much larger than that of M-1 (14.10 vs. 8.65 cm). This indicated that coniferous trees tended to increase the transformation accuracy. For coniferous stands, the accuracy of R-OICP was slightly higher than that of N-OICP (horizontal RMSE: 6.02 vs. 6.55 cm; vertical RMSE: 4.31 vs. 6.78 cm). However, for a mixed broadleaf-coniferous forest, the performances of R-OICP and N-OICP were quite comparative, with similar errors (horizontal MAE: 6.96 vs. 6.70 cm; vertical MAE: 5.64 vs. 5.73 cm; horizontal RMSE: 8.04 vs. 7.86 cm; vertical RMSE: 6.84 vs. 6.93 cm) in both directions. For the broadleaf forest, the RMSE of N-OICP reduced by 2% and 6% compared to that of R-OICP in the horizontal (14.75 vs. 15.04 cm) and vertical (13.42 vs. 14.21 cm) directions, respectively.

It is worth noting that the accuracy in the vertical direction was slightly higher than that in the horizontal direction, with approximately 1 cm lower MAE and RMSE. These results indicated that differential constraints existed in the horizontal and vertical directions. Although optimized algorithms performed variously for different forest types, they were stable and accurate for registering TLS and ULS data.

3.2. Estimation of individual tree parameters using different registration algorithms

3.2.1 Individual tree crown delineation

Based on the U-TLS data registered by the three optimized algorithms (i.e. F-OICP, R-OICP, and N-OICP), the CSP algorithm was conducted to delineate individual trees for the three stand types. The traditional ICP algorithm was also conducted as a baseline. Table 4 shows that all three optimized algorithms outperformed the traditional ICP according to the average recall(r), precision (p), and F-score. F-OICP and R-OICP improved the r over traditional ICP by 4% (0.79 vs. 0.76) and N-OICP improved it by 1% (0.77 vs. 0.76). This was because the U-TLS point cloud registered by the optimized algorithm could describe the actual canopy morphology and the CSP algorithm could detect more 1:1 matched trees. F-OICP and R-OICP improved p by 4% over N-OICP and R-OICP (0.73 vs. 0.70), which indicated that the F-OICP and R-OICP algorithms reduced the number of omitted trees using the CSP algorithm and effectively decreased over-segmentation. The F-OICP algorithm achieved the most accurate F-score, with improvements of 3%, 5%, and 5% over R-OCIP (0.77 vs. 0.75), N-OICP (0.77 vs. 0.73), and ICP (0.77 vs. 0.73), respectively. This indicates that F-OICP can effectively avoid

Table 4. Accuracy assessment of ITCD using CSP algorithm based on U-TLS data registered by different algorithms.

Stand type	Stem density (stems/ha)	Statistics	F-OICP			R-OICP			N-OICP			ICP		
			r	p	F-score	r	p	F-score	r	p	F-score	r	p	F-score
Coniferous	790	Mean	0.81	0.76	0.78	0.81	0.75	0.78	0.79	0.75	0.76	0.79	0.74	0.76
		Std	0.06	0.05	0.07	0.06	0.06	0.06	0.07	0.05	0.06	0.07	0.08	0.08
Mixed	1200	Mean	0.74	0.68	0.71	0.74	0.67	0.70	0.72	0.65	0.68	0.71	0.65	0.68
		Std	0.03	0.03	0.03	0.03	0.02	0.03	0.03	0.03	0.03	0.04	0.04	0.04
Broadleaf	760	Mean	0.83	0.74	0.78	0.81	0.73	0.76	0.81	0.69	0.74	0.79	0.71	0.74
		Std	0.01	0.03	0.03	0.04	0.03	0.03	0.03	0.01	0.03	0.03	0.01	0.01
Mean	-	-	**0.79**	**0.73**	**0.77**	**0.79**	**0.72**	**0.75**	**0.77**	**0.70**	**0.73**	**0.76**	**0.70**	**0.73**
Std	-	-	**0.05**	**0.06**	**0.05**	**0.05**	**0.04**	**0.05**	**0.06**	**0.06**	**0.05**	**0.06**	**0.06**	**0.06**

Note: coniferous: coniferous forests, mixed: mixed broadleaf-coniferous forests, broadleaf: broadleaf forests. Std represent the standard deviation of the accuracy indices for all the plots.

Table 5. The accuracy of estimating individual tree DBH using three optimized algorithms and a traditional ICP algorithm.

		F-OICP			R-OICP			N-OICP			ICP		
Stand type	Statistics	R^2	MAE(cm)	RMSE (cm)	R^2	MAE(cm)	RMSE (cm)	R^2	MAE (cm)	RMSE(cm)	R^2	MAE (cm)	RMSE (cm)
Coniferous	Mean	0.93	0.97	1.57	0.94	0.87	1.61	0.92	1.32	1.85	0.91	1.11	1.98
	Std	0.01	0.17	0.49	0.01	0.24	0.63	0.01	0.85	1.03	0.02	0.20	0.48
Mixed	Mean	0.90	1.18	2.19	0.89	1.16	2.05	0.89	1.17	2.18	0.90	1.51	2.14
	Std	0.02	0.24	0.30	0.01	0.17	0.14	0.02	0.10	0.10	0.01	0.36	0.14
Broadleaf	Mean	0.93	0.85	1.74	0.94	1.01	1.47	0.93	0.86	1.52	0.93	1.40	2.08
	Std	0.01	0.10	0.33	0.01	0.14	0.10	0.02	0.17	0.40	0.01	0.30	0.50
Mean	-	**0.92**	**1.00**	**1.83**	**0.92**	**1.01**	**1.71**	**0.91**	**1.12**	**1.85**	**0.91**	**1.34**	**2.07**
Std	-	**0.02**	**0.22**	**0.44**	**0.03**	**0.21**	**0.46**	**0.03**	**0.51**	**0.64**	**0.02**	**0.30**	**0.38**

Note: Std represent the standard deviation of the accuracy indices for all the plots.

Table 6. Accuracy of estimating tree height using three optimized algorithms and traditional ICP algorithm.

		F-OICP			R-OICP			N-OICP			ICP		
Stand type	Statistics	R^2	MAE (m)	RMSE (m)	R^2	MAE (m)	RMSE (m)	R^2	MAE (m)	RMSE (m)	R^2	MAE (m)	RMSE (m)
Coniferous	Mean	0.87	0.15	0.21	0.86	0.18	0.26	0.86	0.17	0.26	0.75	0.40	0.58
	Std	0.04	0.06	0.09	0.02	0.04	0.08	0.04	0.04	0.08	0.03	0.14	0.20
Mixed	Mean	0.84	0.26	0.37	0.83	0.26	0.41	0.82	0.28	0.40	0.75	0.39	0.52
	Std	0.01	0.05	0.05	0.03	0.05	0.06	0.03	0.06	0.07	0.02	0.11	0.12
Broadleaf	Mean	0.84	0.34	0.44	0.78	0.40	0.50	0.77	0.40	0.51	0.66	0.65	0.84
	Std	0.02	0.04	0.05	0.03	0.04	0.07	0.03	0.04	0.05	0.05	0.08	0.11
Mean	-	**0.85**	**0.25**	**0.34**	**0.82**	**0.28**	**0.39**	**0.82**	**0.31**	**0.39**	**0.72**	**0.48**	**0.65**
Std	-	**0.03**	**0.10**	**0.12**	**0.04**	**0.11**	**0.13**	**0.04**	**0.11**	**0.13**	**0.05**	**0.16**	**0.20**

over- and under-segmentation by effectively reducing crown shift during registration.

For different stand types, the accuracies of ITCD for broadleaf forests were very similar to that for coniferous forests, especially F-OICP (e.g. r: 0.83 vs. 0.81, p: 0.74 vs. 0.76, and F-score: 0.78 vs. 0.78). The mixed broadleaf-coniferous forests obtained the lowest accuracy, but the average F-score was still above 0.68. This could be because the mixed forests had the highest stand density (i.e. 1200 stems/ha) and the dense trunks and overlapping canopies seriously affected individual tree crown delineation.

Overall, the r indices of CSP were higher than the p indices of the corresponding method, indicating that the CSP method tended to detect more false positives than false negatives. In general, the optimized registration algorithms accurately described the location of individual trees and the tree crowns within all stand types compared to the traditional ICP.

3.2.2 Individual tree parameters estimation

The main purpose of this study was to obtain comprehensive 3D structural information and accurately estimate individual tree parameters in dense forest based on precisely registered ULS and TLS data. Therefore, we evaluated the effectiveness of the fused U-TLS data using different optimized registration algorithms in estimating individual tree parameters: DBH and tree height (Tables 5 and 6). The effectiveness using the ICP algorithm was also evaluated as a baseline.

In terms of DBH (Table 5), the fitting accuracy of the optimized registration algorithms was consistent with that of the traditional ICP algorithm (R^2>0.88, RMSE <3.615 cm). Of the four algorithms, the performances of F-OICP, R-OICP, and N-OICP were quite comparative, with similar errors for estimating individual tree DBH (RMSE: F-OICP: 1.13–2.57 cm, R-OICP: 0.99–2.59 cm, N-OICP: 1.11–3.62 cm, ICP: 1.29–2.64 cm) (Supplementary table S3). The optimized coarse-to-fine algorithms did not show any advantages in estimating individual tree DBH compared to the traditional ICP algorithm, which was consistent with the results of the visual evaluation (see Slice **I** of Figure 5). This was because that ULS data barely detected the tree trunk and the DBH was mainly estimated from the TLS data without ULS points. We noticed some extreme values in the N-OICP algorithm (for plot C-4: RMSE of 3.62 cm) (Supplementary table S3), indicating that this algorithm was more prone to generating extreme values than F-OICP (RMSE: 1.26 cm) and R-OICP (RMSE:

0.99 cm), which affected the stability of the registration results.

Coniferous and broadleaf forests achieved the highest and similar accuracy for DBH estimation, while mixed broadleaf-coniferous forests obtained the lowest. The average RMSE of coniferous forests was 40% lower than that of mixed broadleaf-coniferous forests (1.57 vs. 2.19 cm) when using F-OICP, while the RMSE was 11% lower compared to that of broadleaf forests (1.57 vs. 1.74 cm). This was because mixed broadleaf-coniferous and broadleaf forests have abundant shrubs and herbs, which could interfere with DBH extraction accuracy.

On the other hand, the registration algorithms differed greatly in estimating tree height (Table 6). The F-OICP algorithm achieved the highest accuracy ($R^2 = 0.85$, MAE = 0.25 m, RMSE = 0.34 m), followed by R-OICP ($R^2 = 0.82$, MAE = 0.28 m, RMSE = 0.39 m) and N-OICP ($R^2 = 0.82$, MAE = 0.31 m, RMSE = 0.39 m) algorithms, and the lowest accuracies were obtained by the ICP algorithm ($R^2 = 0.72$, MAE = 0.48 m, RMSE = 0.95 m). The average RMSE of the F-OICP algorithm was 91% lower than that of the ICP algorithm (0.34 vs. 0.65), while both R-OICP and N-OICP achieved an RMSE 67% lower than that of the ICP algorithm (0.39 vs. 0.65). This was because the optimized coarse-to-fine algorithms not only provide an accurate initial position by calculating the effective features (e.g. angle and normal) but also effectively avoid local minima that ICP traps into. This result was consistent with previous results on transformation accuracy (Table 3). In general, the optimized algorithms performed well for tree height estimation, with R^2, MAE, and RMSE values of 0.77–0.87, 0.15–0.40, and 0.21–0.51 for all stand types, respectively (Supplementary table S4).

According to stand type, coniferous forests had the highest accuracy (e.g. for F-OICP, R^2: 0.87, MAE: 0.15 m, and RMSE: 0.21 m) in terms of tree height estimation, followed by mixed broadleaf-coniferous (e.g. for F-OICP, R^2: 0.84, MAE: 0.26 m, and RMSE: 0.37 m) and broadleaf (e.g. for F-OICP, R^2: 0.84, MAE: 0.34 m, and RMSE: 0.44 m) forests. For the different stands with similar stem density (for instance, C-4: 930 stems/ha; M-1: 900 stems/ha; B-5: 940 stems/ha), the R^2 of plot C-4 was 10% (0.92 vs. 0.84) and 12% (0.92 vs. 0.82) higher than those of plots M-1 and B-5 using F-OICP, respectively (Supplementary table S4). The RMSE of plot C-4 was 60% (0.18 vs. 0.45) and 64% (0.18 vs. 0.51) lower than those of plots M-1 and B-5 using F-OICP, respectively (Supplementary table S4). The other algorithms had similar trends. This indicated that the mixed broadleaf-coniferous and broadleaf forests had more errors in tree height estimation than coniferous forests.

3.3. ANOVA analysis

To further investigate the statistical significance of various registration algorithms, two-way ANOVA analysis (factors: registration algorithm and stand type) was conducted on the F-score of ITCD (i.e. CSP) and the RMSE of DBH and tree height estimates. Table 7 shows that the algorithm and stand type have no significant interactions effect on ITCD (p-value = 1.0), as well as no significant interaction effect on the estimated DBH and tree height (both p-value = 0.07) at a 5% level of significance. This indicated that the impact of the registration algorithm did not depend on the stand type of the response variable (e.g. F-score and RMSE). Table 7 shows that the main effect of stand type was statistically significant for ITCD, DBH, and tree height estimations (p-value<0.05).

Table 7. Two-way ANOVA of the accuracy indices of ITCD and individual tree parameter estimation.

Parameter	Factor	Degree of freedom	Sum of square	Mean Square	F- statistics	p-value
ITCD	Stand type	2	0.07	0.04	17.39	0.00*
	Algorithm	3	0.01	0.00	1.35	0.26
	Stand type× Algorithm	6	0.00	0.00	0.04	1.00
DBH	Stand type	2	4.22	2.11	10.76	0.00*
	Algorithm	3	0.11	0.04	0.18	0.91
	Stand type× Algorithm	6	2.52	0.42	2.14	0.07
	Stand type	2	0.62	0.31	32.15	0.00*
Tree height	Algorithm	3	0.88	0.29	30.33	0.00*
	Stand type×Algorithm	6	0.12	0.02	2.11	0.07

Note: "*" represents significant differences at $p < 0.05$. The response variables are F-score for ITCD and RMSE for DBH and tree height.

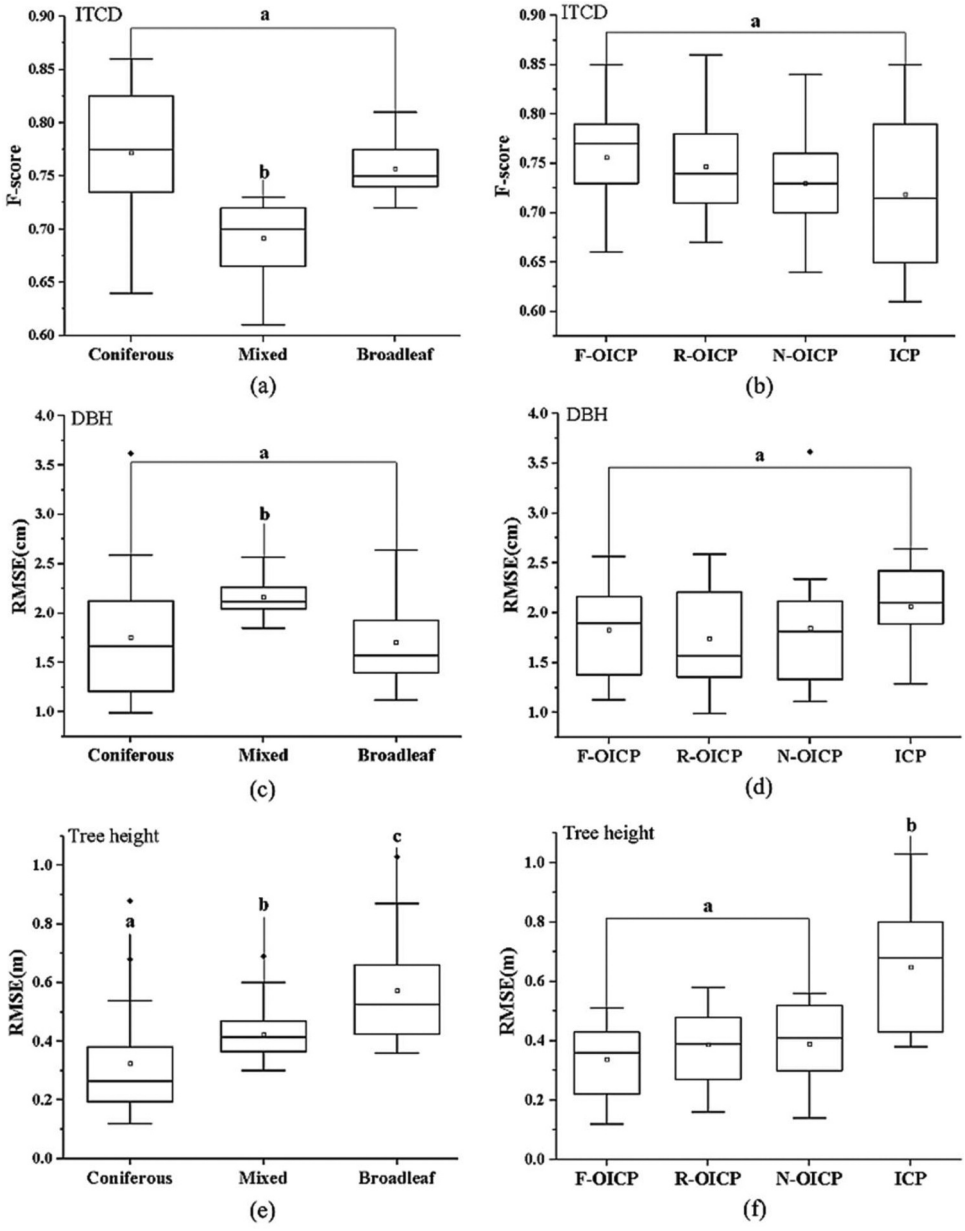

Figure 6. Turkey test for the RMSE of DBH and tree height estimated by different registration algorithms for three stand types. (a) F-score of ITCD; main effect: stand type; (b) F-score of ITCD; main effect: registration algorithm; (c) RMSE of DBH; main effect: stand type; (d) RMSE of DBH; main effect: registration algorithm; (e) RMSE of tree height; main effect: stand type; and (f) RMSE of tree height; main effect: registration algorithm. Different lowercase letters indicate statistical differences using Tukey test post-hoc and significant differences between forest stand type or algorithm. "·" represent the outliers.

However, the registration algorithm only affected the RMSE of tree height (p-value<0.05). This indicated that the algorithms were not statistically significant for the accuracy of DBH and ITCD because the ULS data barely transmitted through the canopy and affected ITCD and the DBH estimation.

It is unclear which algorithm or stand type differs from the others in terms of p-values in Table 7 because ANOVA only tests whether the means of observations grouped by one factor are the same. To identify means that are significantly different from one another, Tukey's HSD test, a multiple comparison approach, was applied (see Figure 6). Figure 6(a,b) showed the main effects of stand type and registration algorithms on the F-score of ITCD. Mixed broadleaf-coniferous forests significantly differed from coniferous and broadleaf forests. This confirmed that stand type had a significant impact on ITCD accuracy, whereas registration algorithm had little impact, although F-OICP had a slightly higher F-score than

the other algorithms. Figure 6(c,d) show the main effects of stand type and registration algorithms on the RMSE of DBH estimates. With a larger RMSE by 2.14 cm, the mixed broadleaf-coniferous forests varied significantly from coniferous to broadleaf forests. This supports the results from Table 7 that stand type had a considerable influence on DBH estimations, whilst registration algorithms had a negligible effect.

On the other hand, Figure 6(e,f) show that stand type and registration algorithm greatly impacted the accuracy of tree height estimations. The tree height of coniferous forests was the most accurate, followed by that of mixed broadleaf-coniferous and broadleaf forests (Figure 6(e)). It is worth noting that the optimized registration algorithms significantly improved tree height estimation compared to traditional ICP. However, there was no significant difference among the three optimized algorithms (Figure 6(f)), except that the accuracy of F-OICP for tree height estimation was slightly better than the other two optimized algorithms (i.e. R-OICP and N-OICP).

4. Discussion

4.1. Strengths of optimized coarse-to-fine algorithms

In this study, we proposed three optimized coarse-to-fine registration algorithms (i.e. F-OICP, R-OICP, and N-OICP) for accurately registering TLS and ULS data to estimate individual tree parameters (DBH and tree height) according to different stand types with tree densities between 400 and 1500 stems/ha. The proposed optimized algorithms provided reliable registration results with small transformation errors (average RMSE of about 9.3 cm). In addition, the accuracy of the three optimized algorithms in the vertical direction was slightly better than that in the horizontal direction (RMSE: 7.37 vs. 8.36 cm). This was because (1) the ground presents a significant constraint on registration in the vertical direction due to the relatively flat topography of the study's sites (elevation: 353–380 m), and (2) in general, canopy penetration can be decomposed into horizontal and vertical directions and saturates at angles of about 27° for UAV-LiDAR system (Liang, Kankare, and Hyyppä 2016). When canopy penetration is unsaturated, the vertical penetration depth is more likely to be greater than the horizontal penetration depth, resulting in more canopy information in the vertical direction. The results were similar to those obtained by Zhang, Shao, and Jin (2021), who obtained twice as much error in the horizontal direction as in the vertical direction in larch plots.

The optimized algorithms produced accurate registration in addition to accurate individual tree parameters, especially tree height. Since using only TLS data in dense forests would considerably underestimate tree height (Wilkes, Lau, and Disney 2017; Wilkes et al. 2018; Terryn, Calders, and Bartholomeus 2022), it is indispensable to combine ULS and TLS for accurate tree height estimation. Well-performing registration algorithms assist in fusing ULS and TLS point data. The three optimized registrations algorithms, F-OICP, R-OICP, and N-OICP, proposed in this study estimated the tree height with relatively low RMSE (0.34, 0.39, and 0.39 m, respectively) compared to that of traditional ICP (0.65 m). The accuracies were similar but slightly higher than those obtained in similar studies. For example, Hauglin et al. (2014) estimated the tree height of Norway spruce (Picea Abies (L.) as the dominant tree species with an RMSE of 0.5–1.0 m based on registered airborne laser scanning (ALS) and TLS data. Polewski et al. (2016) used ALS and terrestrial photogrammetric point clouds in coniferous forests and achieved tree height estimations with an average RMSE of approximately 0.6 m. Terryn, Calders, and Bartholomeus (2022) registered TLS and ULS data using the traditional ICP algorithm for tree height estimations in tropical forests, achieving an average RMSE of 0.4 m. It is worth mentioning that the proposed optimized algorithms were stable and performed well for natural secondary forest with an average density of 910 stems/ha, while the density of the previous studies ranged from 400 to 700 stems/ha. This indicated that the optimizing strategy (e.g. coarse-to-fine registration, accelerating and optimizing ICP iterations) we designed was effective for registering ULS and TLS.

The three coarse registration algorithms (FPFH, RANSAC, and NDT) describe the point cloud morphological structure using different strategies: FPFH extracts geometric relationships within a specific range (i.e. the angular difference between the normal vector of two points and their adjacent points); RANSAC selects a large number of robust minimum point cloud subsets; NDT calculates the point cloud normal distribution structure. The advantage of F-OICP is that it can capture the leaf orientation and

Table 8. Runtime performance of the registration algorithms.

		Number of Points		Runtime (second)			
Stand type	Statistics	TLS	ULS	F-OICP	R-OICP	N-OICP	ICP
Coniferous	Mean	44853920	196118	236.0	230.4	251.4	396.5
	Std	-	-	39.9	22.3	32.7	17.9
Mixed	Mean	52555915	215341	302.5	315.4	331.5	411.7
	Std	-	-	17.0	29.5	21.5	12.1
Broadleaf	Mean	41060974	242423	218.8	222.3	224.1	385.1
	Std	-	-	53.6	53.6	52.9	19.5
Mean	-	**46156936**	**217960**	**252.4**	**256.1**	**269.0**	**397.8**
Std	-	-	-	**52.7**	**59.4**	**59.1**	**29.3**

Note: The number of TLS point clouds is the total amount of resampled point clouds.

canopy distribution because the FPFH descriptor consisting of normal vectors is highly correlated with the 3D distribution of leaf orientations and the leaf angle PDF (Bailey and Mahaffee 2017; Dai et al. 2019). Thus, among the three optimized registration algorithms, F-OICP performed slightly better than R-OICP and N-OICP in terms of transformation accuracy (vertical F-OICP: 7.73 m; R-OICP: 8.45 cm; N-OICP: 9.04 cm) and tree height (F-OICP: 0.34 m; R-OICP and N-OICP: 0.39 m). The RMSE of F-OICP was noticeably lower than those obtained in past studies of coniferous forests conducted by Polewski et al. (2019) and Zhang, Shao, and Jin (2021), who obtained RMSEs of tree height of 0.36 and 0.42 m, respectively. This may be attributed to the accurate feature description of the canopy of the F-OICP algorithm (Zhang et al. 2021; Wang et al. 2022). Notably, the RMSE of the F-OICP algorithm was only 0.12 m for plot C-5 (Supplementary table S4). The small error may come from the wind, noise, and systematic errors of the UAV-LiDAR system (Dai et al. 2019; Schneider, Kükenbrink, and Schaepman 2019; Calders et al. 2020). It is of great significance that the proposed optimized algorithm (e.g. F-OICP) can be fully applied to the refined individual tree parameter (e.g. tree height) survey of various dense forests, especially coniferous forests.

The proposed optimized algorithms did not require any parameters except for the downsampling voxel size and the iteration termination condition of the optimized ICP (i.e. ε: the threshold for the minimum distance between the source point and the target point). The runtime performance of the optimized coarse-to-fine algorithms and traditional ICP algorithm are compared in Table 8.

In contrast to traditional ICP, the average run times of the optimized coarse-to-fine algorithms were approximately 54% lower (ICP vs. F-OICP, R-OICP, N-OICP: 397.8 s vs. 252.4 s, 256.1 s, 269.0 s). Therefore, the proposed optimized algorithms not only improved the accuracy of tree height estimates but also sped up registration convergence. This was due to the optimized algorithms' ability to create initial positions for fine registration rapidly and accurately through coarse registration. This technique boosted the likelihood of escaping from local minima while simultaneously reducing the number of repetitive computations. Furthermore, the CAS algorithm resulted in a significant reduction in overall runtime by improving the operational efficiency of the coarse registration. Another advantage of the optimized registration algorithms was that the KD-tree algorithm improved the efficiency and accuracy compared to the ICP algorithm by optimizing the technology of the ICP algorithm to reconfigure the storage space of the point clouds and calculate the nearest points (Zhang 2016). To the best of our knowledge, most existing studies that successfully registered forest TLS and ULS data were time consuming. For example, Kelbe, Aardt, and Romanczyk (2016) and Dai et al. (2019) implemented the registration of TLS and ULS in 32×32 m plots (the total number of points in the plots reached 130,000), with an average execution time of 10.8 min. Thus, it is promising to apply the optimized algorithms (especially F-OICP) to register TLS and ULS accurately and efficiently for dense forests in the future.

4.2. Effect of stand type on individual tree parameters estimation

The stand type significantly influenced the transformation accuracy of the registration algorithm, individual tree crown delineation, and individual tree parameter estimation. It is evident that coniferous forests (average of RMSE: 3.38 cm) obtained the highest transformation accuracy compared to mixed

broadleaf-coniferous (average of RMSE: 6.34 cm) and broadleaf (average of RMSE: 12.37 cm) forests. The accuracies were much higher than those obtained by Polewski et al. (2019), which achieved a mean transformation deviation of 27–36 cm for three coniferous plots and 54–67 cm for four broadleaf plots based on registered UAV and backpack LiDAR point clouds. Coniferous forests typically have better accuracy because they have more regular leaf morphology and crown profiles than broadleaf forests, which results in stable features and strict constraints for the registration algorithm.

An accurate individual tree crown delineation algorithm is the basis and prerequisite for a precise forest structure estimate (Næsset et al. 2016). In this study, the CSP algorithm was applied to delineate the individual tree crown using registered U-TLS data. The accuracies for coniferous and broadleaf forests were slightly higher than those for mixed broadleaf-coniferous forests. The F-score for ITCD in the coniferous forests (about 0.8) was significantly higher than that obtained in a previous study (Zhen et al. 2022), which reported an average F-score of 0.6 using 1:1 matched tree based on ULS and backpack laser scanning (BLS) data. The F-score for ITCD (i.e. 0.74–0.81) (Supplementary table S2) was similar to that obtained by Huo, Lindberg, and Holmgren (2022), who obtained an F-score of 0.76–0.85 in a dense broadleaf forests.

The stand type greatly influenced the accuracy of individual tree parameter estimation. The accuracy of DBH estimates of coniferous and broadleaf forests was better than that of mixed broadleaf-coniferous forests (F-OICP RMSE: 1.57 and 1.74 cm vs. 2.19 cm). This was because the tree density of mixed broadleaf-coniferous forests was higher (about 1160 stems/ha) than the other stand types and the mixed broadleaf-coniferous forests had abundant shrubs and herbs, which could interfere with DBH extraction accuracy. Although TLS has advantages for DBH estimation in dense forests, the greater the tree density, the more likely the trunk is occluded, resulting in a decrease in DBH estimation accuracy (Kükenbrink, Schneider, and Leiterer 2017; Li, Xu, and Wu 2022). It is worth noting that stand type significantly influenced the accuracy of tree height estimation. The tree height estimation of coniferous forests (F-OICP RMSE: 0.21 m) was the most accurate, followed by those of mixed broadleaf-coniferous (F-OICP RMSE: 0.37 m) and broadleaf (F-OICP RMSE: 0.44 m) forests. This was because coniferous trees have obvious apical or umbrella structures compared to broadleaf trees. Reliable height measurements require point spacing at a 1–2 cm level at the treetops, which allows for the possibility of obtaining a hit on small top branches (i.e. the branches connected to leaves) (Liang, Kankare, and Hyyppä 2016; Calders et al. 2020). Thus, the sparse canopy of conifers formed by the apical structure and needle-shaped leaves is susceptible to capture by ULS, which will provide more canopy details to the optimized algorithm than broadleaf trees (Mcintyre 1964; Cline and Deppong 1999; Barbier, Dun, and Beveridge 2017; Ren and Wu 2020).

4.3. Limitations

Although the optimized coarse-to-fine algorithms are promising registration algorithms, there are still certain limitations. First, the optimized algorithms were proposed and tested using small-scale plots (i.e. 30 × 30 m) in natural secondary forests of northern China. To improve the generalizability of the algorithms, it is necessary to test the efficiency on large plots (e.g. 100 × 100 m) in other forests, such as southern forests and tropical forests. First, despite being an automated, parameter-free registration algorithm, the improved algorithms are still susceptible to internal parameters (such as the voxel size of the downsampled), which will affect their registration accuracy. In the future, automatic iteration should be applied to choose the best parameters. Second, although the registration algorithms significantly impacted the tree height estimates, there was no significant difference in the ITCD and DBH estimation. However, all the optimized algorithms showed superior DBH accuracy for all stand types (i.e. R^2>0.86, RMSE<3.62 cm). In coniferous forests, the F-OICP algorithm still performed better than the R-OICP and N-OICP algorithms in terms of registration and ITC segmentation (e.g. RMSE of tree height F-OICP: 0.34, R-OICP: 0.39, N-OICP: 0.39; F-score F-OICP: 0.77, R-OICP: 0.75, N-OICP: 0.73). Finally, the transferability of the algorithms on platforms has not been explored. It is expected that the registration algorithms could be used for LiDAR data on other platforms, such as the fusion of ULS and BLS or ULS and mobile laser scanning (MLS). With the increase of applications of ULS and TLS data in forestry, more work should be devoted to providing stable and efficient registrations

for refined forest inventories, including improving the accuracy of individual tree parameter estimation, which would provide a sound foundation for accurately estimating forest biomass and carbon stock.

5. Conclusions

The growing demand for fine individual tree parameters requires more accurate and efficient registration on a variety of LiDAR platforms. This study contributed to developing an automated, nearly parameter-free, and efficient registration algorithm to integrate multi-platform LiDAR point data (e.g. ULS and TLS) for improving the accuracy of individual tree parameters (i.e. DBH and tree height) in dense forests (i.e. natural secondary forest). The optimized coarse-to-fine registration algorithms (i.e. F-OICP, R-OICP, and N-OICP) achieved good performances in registration accuracy, ITC segmentation, individual tree parameter estimation, and efficiency. In particular, F-OICP achieves the highest accuracy of tree height estimation in coniferous forests. The other improved algorithms (R-OICP and N-OICP) can also be applied for registration toward ITCD and individual tree parameters estimation in dense forests. However, the performances of these algorithms on other forest types (e.g. tropical forests and southern forests) for diverse LiDAR platform data (e.g. ULS, BLS, and MLS) should be further investigated. The optimized registration algorithms can facilitate the synergistic utilization of multi-platform LiDAR and provide appealing and promising methods for accurate quantification of individual tree parameters, efficient forest inventories, precise forest monitoring and protection, and sustainable forest management.

Disclosure statement

No potential conflict of interest was reported by the authors.

Funding

This work was supported by the Fundamental Research Funds for the Central Universities [2572020BA05]; National Natural Science Foundation of China [32071677]; National Natural Science Foundation of China [31870530]; National Forestry and Grassland Data Center-Heilongjiang platform [2005DKA32200-OH]; R&D Program for Forest Science Technology (Project No. (FTIS 2020179A00-2022-BB01) provided by Korea Forest Service(Korea Forestry Promotion Institute); Korea Environment Industry & Technology Institute (KEITI) through its Urban Ecological Health Promotion Technology Development Project and funded by the Korea Ministry of Environment (MOE) [2020002770001]

ORCID

Zhen zhen http://orcid.org/0000-0001-9281-4260

Data availability statement

The data that support the findings of this study are openly available in [figshare] at [https://doi.org/10.6084/m9.figshare.21786140.v1]. The reference data are available on request from the corresponding authors (Z.Z. and Y.Z.).

References

Aiger, D., N. J. Mitra, and D. Cohen-Or. 2008. "4-Points Congruent Sets for Robust Pairwise Surface Registration." *ACM Transactions on Graphics* 27 (3): 1–10. doi:10.1145/1360612.1360684.

Almeida, C. T., L. S. Galvão, L. E. O. C. Aragão, J. P. H. B. Ometto, A. D. Jacon, F. R. D. S. Pereira, L. Y. Sato, et al. 2019. "Combining LiDar and Hyperspectral Data for Aboveground Biomass Modeling in the Brazilian Amazon Using Different Regression Algorithms." *Remote Sensing of Environment* 232: 111323. doi:10.1016/j.rse.2019.111323.

Bailey, B. N., and W. F. Mahaffee. 2017. "Rapid Measurement of the Three-Dimensional Distribution of Leaf Orientation and the Leaf Angle Probability Density Function Using Terrestrial LiDar Scanning." *Remote Sensing of Environment* 194: 63–76. doi:10.1016/j.rse.2017.03.011.

Balsi, M., S. Esposito, P. Fallavollita, and C. Nardinocchi. 2018. "Single-Tree Detection in High-Density LiDar Data from UAV-Based Survey." *European Journal of Remote Sensing* 51 (1): 679–692. doi:10.1080/22797254.2018.1474722.

Barbier, F. F., E. A. Dun, and C. A. Beveridge. 2017. "Apical Dominance." *Current Biology* 27 (17): 864–865. doi:10.1016/j.cub.2017.05.024.

Bentley, L. P., J. C. Stegen, V. M. Savage, and D. D. Smith. 2013. "An Empirical Assessment of Tree Branching Networks and Implications for Plant Allometric Scaling Models." *Ecology Letters* 16 (8): 1069–1078. doi:10.1111/ele.12127.

Besl, P., and H. D. McKay. 1992. "A Method for Registration of 3-D Shapes." *IEEE Transactions on Pattern Analysis and Machine Intelligence* 14 (2): 239–256. doi:10.1109/34.121791.

Biber, P., and W. G. Straßer. 2003. "The Normal Distributions Transform: A New Approach to Laser Scan Matching." *2003 IEEE RSJ International Conference on Intelligent Robots and Systems* 3.doi: 10.1109/IROS.2003.1249285.

Bouaziz, S., A. Tagliasacchi, and M. Pauly. 2013. "Sparse Iterative Closest Point." *Computer Graphics Forum* 32 (5): 113–123. doi:10.1111/cgf.12178.

Brede, B., K. Calders, A. Lau, P. Raumonen, H. M. Bartholomeus, M. Herold, and L. Kooistra. 2019. "Non-Destructive Tree Volume Estimation Through Quantitative Structure Modelling: Comparing UAV Laser Scanning with Terrestrial LIDAR." *Remote Sensing of Environment* 223: 111355. doi:10.1016/j.rse.2019.111355.

Calders, K., J. S. Adams, J. Armston, and H. Bartholomeus. 2020. "Terrestrial Laser Scanning in Forest Ecology: Expanding the Horizon." *Remote Sensing of Environment* 251: 112102. doi:10.1016/j.rse.2020.112102.

Calders, K., J. Armston, and G. Newnham. 2014. "Implications of Sensor Configuration and Topography on Vertical Plant Profiles Derived from Terrestrial LiDar." *Agricultural and Forest Meteorology* 194: 104–117. doi:10.1016/j.agrformet.2014.03.022.

Chambers, J. Q., G. P. Asner, and D. C. Morton. 2007. "Regional Ecosystem Structure and Function: Ecological Insights from Remote Sensing of Tropical Forests." *Trends in Ecology & Evolution* 22 (8): 414–423. doi:10.1016/j.tree.2007.05.001.

Choi, H., and S. Youngkeun. 2022. "Comparing Tree Structures Derived Among Airborne, Terrestrial and Mobile LiDar Systems in Urban Parks." *GIScience & Remote Sensing* 59 (1): 843–860. doi:10.1080/15481603.2022.2076381.

Chum, O., J. Matas, and J. Kittler. 2003. "Locally Optimized RANSAC." *DAGM-Symposium Pattern Recognition* 236–243. doi: 10.1007/978-3-540-45243-0.31.

Chung, C.H., W. Chao-Huan, H. Han-Ching, and H. Cho-Ying. 2019. "Comparison of Forest Canopy Height Profiles in a Mountainous Region of Taiwan Derived from Airborne Lidar and Unmanned Aerial Vehicleimagery." *GIScience & Remote Sensing* 56 (8): 1289–1304. doi:10.1080/15481603.2019.1627044.

Cline, M. G., and D. O. Deppong. 1999. "The Role of Apical Dominance in Paradormancy of Temperate Woody Plants: A Reappraisal." *Journal of Plant Physiology* 155 (3): 350–356. doi:10.1016/S0176-1617(99)80116-3.

Dai, W. X., B. S. Yang, X. L. Liang, and Z. Dong. 2019. "Automated Fusion of Forest Airborne and Terrestrial Point Clouds Through Canopy Density Analysis." *ISPRS Journal of Photogrammetry and Remote Sensing* 156 (11): 94–107. doi:10.1016/j.isprsjprs.2019.08.008.

Dong, Z., F. X. Liang, and B. S. Yang. 2020. "Registration of Large-Scale Terrestrial Laser Scanner Point Clouds: A Review and Benchmark." *ISPRS Journal of Photogrammetry and Remote Sensing* 163: 327–342. doi:10.1016/j.isprsjprs.2020.03.013.

Du, C. Y., W. Y. Fan, Y. Ma, H. Jin, and Z. Zhen. 2021. "The Effect of Synergistic Approaches of Features and Ensemble Learning Algorithm on Aboveground Biomass Estimation of Natural Secondary Forests Based on ALS and Landsat 8." *Sensors* 21 (17): 5974. doi:10.3390/s21175974.

Ewald, M., R. Aerts, J. Lenoir, F. E. Fassnacht, M. Nicolas, S. Skowronek, J. Piat, et al. 2018. "LiDar Derived Forest Structure Data Improves Predictions of Canopy N and P Concentrations from Imaging Spectroscopy." *Remote Sensing of Environment* 211: 13–25. doi:10.1016/j.rse.2016.07.023.

Fang, F., J. Im, J. Lee, and K. Kim. 2016. "An Improved Tree Crown Delineation Method Based on Live Crown Ratios from Airborne LiDar Data." *GIScience & Remote Sensing* 53 (3): 402–419. doi:10.1080/15481603.2016.1158774.

Fischler, M. A., and R. C. Bolles. 1987. "Random Sample Consensus: A Paradigm for Model Fitting with Applications to Image Analysis and Automated Cartography." *Readings in Computer Vision* 24 (6): 381–395. doi:10.1145/358669.358692.

Fleck, S., I. Mölder, and M. Jacob. 2011. "Comparison of Conventional Eight-Point Crown Projections with LIDAR-Based Virtual Crown Projections in a Temperate Old-Growth Forest." *Annals of Forest Science* 68 (7): 1173–1185. doi:10.1007/s13595-011-0067-1.

Gara, T. W., A. K. Skidmore, R. Darvishzadeh, and T. J. Wang. 2019. "Leaf to Canopy Upscaling Approach Affects the Estimation of Canopytraits." *GIScience & Remote Sensing* 56 (4): 554–575. doi:10.1080/15481603.2018.1540170.

Greenspan, M., and M. Yurick. 2003. "Approximate K-D Tree Search for Efficient ICP." *Fourth International Conference on 3-D Digital Imaging and Modeling*, *2003*. *3DIM 2003*doi: 10.1109/IM.2003.1240280.

Hartling, S., V. Sagan, and M. Maimaitijiang. 2021. "Urban Tree Species Classification Using UAV-Based Multi-Sensor Data Fusion and Machine Learning." *GIScience & Remote Sensing* 58 (8): 1250–1275. doi:10.1080/15481603.2021.1974275.

Hauglin, M., V. Lien, E. Næsset, and T. Gobakken. 2014. "Geo-Referencing Forest Field Plots by Co-Registration of Terrestrial and Airborne Laser Scanning Data." *International Journal of Remote Sensing* 35 (9): 3135–3149. doi:10.1080/01431161.2014.903440.

Huang, H. B., Z. Li, and P. Gong. 2011. "Automated Methods for Measuring DBH and Tree Heights with a Commercial Scanning Lidar." *Photogrammetric Engineering and Remote Sensing* 77 (3): 219–227. doi:10.14358/PERS.77.3.219.

Huo, L. N., E. Lindberg, and J. Holmgren. 2022. "Towards Low Vegetation Identification: A New Method for Tree Crown Segmentation from LiDar Data Based on a Symmetrical Structure Detection Algorithm (SSD)." *Remote Sensing of Environment* 270: 112857. doi:10.1016/j.rse.2021.112857.

Hyyppä, J., M. Holopainen, and H. Olsson. 2012. "Laser Scanning in Forests." *Remote Sensing* 4 (10): 2919–2922. doi:10.3390/rs4102919.

Jing, L. H., B. X. Hu, T. Noland, and J. L. Li. 2012. "An Individual Tree Crown Delineation Method Based on Multi-Scale Segmentation of Imagery." *ISPRS Journal of Photogrammetry and Remote Sensing* 70 (88): 98. doi:10.1016/j.isprsjprs.2012.04.003.

Jin, S. C., X. L. Sun, F. F. Wu, and Y. J. Su. 2021. "Lidar Sheds New Light on Plant Phenomics for Plant Breeding and Management: Recent Advances and Future Prospects." *ISPRS Journal of Photogrammetry and Remote Sensing* 171: 202–223. doi:10.1016/j.isprsjprs.2020.11.006.

Kelbe, D., J. V. Aardt, and P. Romanczyk. 2016. "Marker-Free Registration of Forest Terrestrial Laser Scanner Data Pairs with Embedded Confidence Metrics." *IEEE Transactions on*

Geoscience and Remote Sensing 54 (7): 4314–4330. doi:10.1109/TGRS.2016.2539219.

Kükenbrink, D., F. D. Schneider, and R. Leiterer. 2017. "Quantification of Hidden Canopy Volume of Airborne Laser Scanning Data Using a Voxel Traversal Algorithm." *Remote Sensing of Environment* 194: 424–436. doi:10.1016/j.rse.2016.10.023.

Le Noë, J., K. H. Erb, S. Matej, A. Magerl, M. Bhan, and S. Gingrich. 2021. "Altered Growth Conditions More Than Reforestation Counteracted Forest Biomass Carbon Emissions 1990–2020." *Nature Communications* 12: 6075. doi:10.1038/s41467-021-26398-2.

Liang, X. L., and J. Hyyppä. 2013. "Automatic Stem Mapping by Merging Several Terrestrial Laser Scans at the Feature and Decision Levels." *Sensors* 13 (2): 1614–1634. doi:10.3390/s130201614.

Liang, X. L., V. Kankare, and J. Hyyppä. 2016. "Terrestrial Laser Scanning in Forest Inventories." *ISPRS Journal of Photogrammetry and Remote Sensing* 115: 63–77. doi:10.1016/j.isprsjprs.2016.01.006.

Li, W. K., Q. H. Guo, M. K. Jakubowski, and M. Kelly. 2012. "A New Method for Segmenting Individual Trees from the Lidar Point Cloud." *Photogrammetric Engineering and Remote Sensing* 78 (1): 75–84. doi:10.14358/PERS.78.1.75.

Liu, S. L., F. Y. Cheng, S. K. Dong, H. D. Zhao, X. Hou, and X. Wu. 2017. "Spatiotemporal Dynamics of Grassland Aboveground Biomass on the Qinghai-Tibet Plateau Based on Validated MODIS NDVI." *Scientific Reports* 7: 4182. doi:10.1038/s41598-017-04038-4.

Li, S. H., J. X. Wang, Z. Q. Liang, and L. Su. 2016. "Tree Point Clouds Registration Using an Improved ICP Algorithm Based on Kd-Tree." 2016 IEEE International Geoscience and Remote Sensing Symposium (IGARSS) doi: 10.1109/IGARSS.2016.7730186.

Li, P., R. S. Wang, Y. X. Wang, and W. Y. Tao. 2020. "Evaluation of the ICP Algorithm in 3D Point Cloud Registration." *IEEE Access* 8: 68030–68048. doi:10.1109/ACCESS.2020.2986470.

Li, Y. T., X. Xu, and Z. Z. Wu. 2022. "A Forest Type-Specific Threshold Method for Improving Forest Disturbance and Agent Attribution Mapping." *GIScience & Remote Sensing* 59 (1): 1624–1642. doi:10.1080/15481603.2022.2127459.

Lowe, D. G. 2004. "Distinctive Image Features from Scale-Invariant Keypoints." *International Journal of Computer Vision* 60 (2): 91–110. doi:10.1023/B:VISI.0000029664.99615.94.

Lu, W. X., G. W. Wan, and Y. Zhou. 2019. "DeepVcp: An End-To-End Deep Neural Network for Point Cloud Registration." *2019 IEEE/CVF International Conference on Computer Vision (ICCV)* 12–21. doi: 10.1109/ICCV.2019.00010.

Madec, S., F. Baret, B. Solan, and S. Thomas. 2017. "High-Throughput Phenotyping of Plant Height: Comparing Unmanned Aerial Vehicles and Ground LiDar Estimates." *Frontiers in Plant Science* 8: 2002. doi:10.3389/fpls.2017.02002.

Magnusson, M. 2009. "The Three-Dimensional Normal-Distributions Transform — an Efficient Representation for Registration, Surface Analysis, and Loop Detection." *Computer Science*.

Magnusson, M., H. Andreasson, A. Nuchter, and A. J. Lilienthal. 2009. "Appearance-Based Loop Detection from 3D Laser Data Using the Normal Distributions Transform." *2009 IEEE International Conference on Robotics and Automation* 26:11–12. doi: 10.1109/ROBOT.2009.5152712.

Mcintyre, G. 1964. "Mechanism of Apical Dominance in Plants." *Nature* 203: 1190–1191. doi:10.1038/2031190a0.

Mellado, N., D. Aiger, and N. J. Mitra. 2014. "Super 4PCS Fast Global Pointcloud Registration via Smart Indexing." *Computer Graphics Forum* 33 (5): 205–215. doi:10.1111/cgf.12446.

Morsdorf, F., D. Ku¨kenbrink, F. D. Schneider, M. Abegg, and M. E. Schaepman. 2018. "Close-Range Laser Scanning in Forests: Towards Physically Based Semantics Across Scales." *Interface Focus: A Theme Supplement of Journal of the Royal Society Interface* 8 (2): 20170046. doi:10.1098/rsfs.2017.0046.

Moskal, L. M., and G. Zheng. 2012. "Retrieving Forest Inventory Variables with Terrestrial Laser Scanning (TLS) in Urban Heterogeneous Forest." *Remote Sensing* 4 (1): 1–20. doi:10.3390/rs4010001.

Næsset, E., H. Ole Ørka, S. Solberg, and O. M. Bollandsås. 2016. "Mapping and Estimating Forest Area and Aboveground Biomass in Miombo Woodlands in Tanzania Using Data from Airborne Laser Scanning, TanDEM-X, RapidEye, and Global Forest Maps: A Comparison of Estimated Precision." *Remote Sensing of Environment* 175: 282–300. doi:10.1016/j.rse.2016.01.006.

Nüchter, A., K. Lingemann, and J. Hertzberg. 2007. "Cached K-D Tree Search for ICP Algorithms." *Sixth International Conference on 3-D Digital Imaging and Modeling (3DIM 2007)* 21–23. doi: 10.1109/3DIM.2007.15.

Nunes, M. H., J. L. C. Camargo, G. Vincent, K. Calders, R. S. Oliveira, A. Huete, Y. Mendes de Moura, et al. 2022. "Forest Fragmentation Impacts the Seasonality of Amazonian Evergreen Canopies." *Nature Communications* 13: 917. doi:10.1038/s41467-022-28490-7.

Paris, C., D. Kelbe, J. V. Aardt, and L. Bruzzone. 2017. "A Novel Automatic Method for the Fusion of ALS and TLS LiDar Data for Robust Assessment of Tree Crown Structure." *IEEE Transactions on Geoscience and Remote Sensing* 55 (7): 3679–3693. doi:10.1109/TGRS.2017.2675963.

Polewski, P., A. Erickson, W. Yao, N. Coops, P. Krzystek, and U. Stilla. 2016. "Object Based Coregistration of Terrestrial Photogrammetric Als Point Clouds in Forested Areas." *ISPRS Annals of the Photogrammetry, Remote Sensing and Spatial Information Sciences* 3: 347–354. doi:10.5194/isprsannals-III-3-347-2016.

Polewski, P., W. Yao, L. Cao, and S. Gao. 2019. "Marker-Free Co-Registration of UAV and Backpack LiDar Point Clouds in Forested Areas." *ISPRS Journal of Photogrammetry and Remote Sensing* 147: 307–318. doi:10.1016/j.isprsjprs.2018.11.020.

Prendes, C., C. Cabo, C. Ordoñez, J. Majada, and E. Canga. 2021. "An Algorithm for the Automatic Parametrization of Wood Volume Equations from Terrestrial Laser Scanning Point Clouds: Application in *Pinus Pinaster*." *GIScience & Remote Sensing* 58 (7): 1130–1150. doi:10.1080/15481603.2021.1972712.

Pyörälä, J., N. Saarinen, and V. Kankare. 2019. "Variability of Wood Properties Using Airborne and Terrestrial Laser Scanning." *Remote Sensing of Environment* 235 (9): 111474. doi:10.1016/j.rse.2019.111474.

Raguram, R., O. Chum, and M. Pollefeys. 2013. "USAC: A Universal Framework for Random Sample Consensus." *IEEE Transactions on Pattern Analysis and Machine Intelligence* 35 (8): 2022–2038. doi:10.1109/TPAMI.2012.257.

Ren, T. Y., and W. C. Wu. 2020. "An Acceleration Algorithm of 3D Point Cloud Registration Based on Iterative Closest Point." *2020 Asia-Pacific Conference on Image Processing, Electronics and Computers (IPEC)* 271–276. doi: 10.1109/IPEC49694.2020.9114965.

RIEGL, 2020.RiSCAN PRO. http://www.riegl.com .

Rusu, R. B. 2010. "Semantic 3D Object Maps for Everyday Manipulation in Human Living Environments." *KI – Ku nstliche Intelligenz* 24 (4): 345–348. doi:10.1007/s13218-010-0059-6.

Rusu, R. B., N. Blodow, and M. Beetz. 2009. "Fast Point Feature Histograms (FPFH) for 3D Registration." *2009 IEEE International Conference on Robotics and Automation* doi: 10.1109/ROBOT.2009.5152473.

Rusu, R. B., Z. C. Marton, N. Blodow, and M. Beetz. 2008. "Persistent Point Feature Histograms for 3D Point Clouds." *Computer Science*. doi:10.3233/978-1-58603-887-8-119.

Santamaría, J., O. Cordón, and S. Damas. 2011. "A Comparative Study of State-Of-The-Art Evolutionary Image Registration Methods for 3D Modeling." *Computer Vision and Image Understanding* 115 (9): 1340–1354. doi:10.1016/j.cviu.2011.05.006.

Schneider, F. D., D. Kükenbrink, and M. E. Schaepman. 2019. "Quantifying 3D Structure and Occlusion in Dense Tropical and Temperate Forests Using Close-Range LiDar." *Agricultural and Forest Meteorology* 268: 249–257. doi:10.1016/j.agrformet.2019.01.033.

Shen, X., and L. Cao. 2017. "Tree-Species Classification in Subtropical Forests Using Airborne Hyperspectral and LiDar Data." *Remote Sensing* 9 (11): 1180. doi:10.3390/rs9111180.

Shenkin, A. F., C. J. Chandler, D. S. Boyd, T. Jackson, M. Disney, N. Majalap, R. Nilus, et al. 2019. "The World's Tallest Tropical Tree in Three Dimensions." *Frontiers in Forests and Global Change* 2: 32. doi:10.3389/ffgc.2019.00032.

Su, Y. T., J. Bethel, and S. Hu. 2016. "Octree-Based Segmentation for Terrestrial LiDar Point Cloud Data in Industrial Applications." *ISPRS Journal of Photogrammetry and Remote Sensing* 113: 59–74. doi:10.1016/j.isprsjprs.2016.01.001.

Tao, S. L., F. F. Wu, Q. H. Guo, and Y. C. Wang. 2015. "Segmenting Tree Crowns from Terrestrial and Mobile LiDar Data by Exploring Ecological Theories." *ISPRS Journal of Photogrammetry and Remote Sensing* 110: 66–76. doi:10.1016/j.isprsjprs.2015.10.007.

Terryn, L., K. Calders, and H. Bartholomeus. 2022. "Quantifying Tropical Forest Structure Through Terrestrial and UAV Laser Scanning Fusion in Australian Rainforests." *Remote Sensing of Environment* 271: 112912. doi:10.1016/j.rse.2022.112912.

Theiler, P. W., J. D. Wegner, and K. Schindler. 2015. "Globally Consistent Registration of Terrestrial Laser Scans via Graph Optimization." *ISPRS Journal of Photogrammetry and Remote Sensing* 109: 126–138. doi:10.1016/j.isprsjprs.2015.08.007.

Wallace, L., R. Musk, and A. Lucieer. 2014. "An Assessment of the Repeatability of Automatic Forest Inventory Metrics Derived from UAV-Borne Laser Scanning Data." *IEEE Transactions on Geoscience and Remote Sensing* 52 (11): 7160–7169. doi:10.1109/TGRS.2014.2308208.

Wang, M., J. Im, Y. H. Zhao, and Z. Zhen. 2022. "Multi-Platform LiDar for Non-Destructive Individual Aboveground Biomass Estimation for Changbai Larch (*Larix Olgensis Henry*) Using a Hierarchical Bayesian Approach." *Remote Sensing* 14 (17): 4361. doi:10.3390/rs14174361.

Wang, Y., and J. M. Solomon. 2019. "Deep Closest Point: Learning Representations for Point Cloud Registration." *2019 IEEE/CVF International Conference on Computer Vision (ICCV)* 3523. doi: 10.1109/ICCV.2019.00362.

Wang, Y. J., C. J. Yan, Y. T. Feng, and S. Y. Du. 2022. "STORM: Structure-Based Overlap Matching for Partial Point Cloud Registration." *IEEE Transactions on Pattern Analysis and Machine Intelligence* 1. doi: 10.1109/TPAMI.2022.3148308.

West, G. B., J. H. Brown, and B. J. Enquist. 1999. "The Fourth Dimension of Life: Fractal Geometry and Allometric Scaling of Organisms." *Science* 284 (5420): 1677–1679. doi:10.1126/science.284.5420.1677.

Wilkes, P., M. Disney, M. B. Vicari, K. Calders, and A. Burt. 2018. "Estimating Urban Above Ground Biomass with Multi-Scale LiDar." *Carbon Balance and Management* 13 (1). doi:10.1186/s13021-018-0098-0.

Wilkes, P., A. Lau, and M. Disney. 2017. "Data Acquisition Considerations for Terrestrial Laser Scanning of Forest Plots." *Remote Sensing of Environment* 196: 140–153. doi:10.1016/j.rse.2017.04.030.

Xu, Q. J., X. D. Sun, C. Y. Wu, P. Q. Wang, and U. Neumann. 2020. "Grid-GCN for Fast and Scalable Point Cloud Learning." *2020 IEEE/CVF Conference on Computer Vision and Pattern Recognition (CVPR)* 5661–5670. doi: 10.1109/CVPR42600.2020.00570.

Yang, Q. L., Y. J. Su, S. C. Jin, and M. Kelly. 2019. "The Influence of Vegetation Characteristics on Individual Tree Segmentation Methods with Airborne LiDar Data." *Remote Sensing* 11 (23): 2880. doi:10.3390/rs11232880.

Yépez-Rincon, F. D., L. Luna-Mendoza, N. L. Ramírez-Serrato, and A. Hinojosa. 2021. "Assessing Vertical Structure of an Endemic Forest in Succession Using Terrestrial Laser Scanning (TLS). Case Study: Guadalupe Island." *Remote Sensing of Environment* 263 (15): 112563. doi:10.1016/j.rse.2021.112563.

Yrttimaa, T., N. Saarinen, and V. Luoma. 2019. "Detecting and Characterizing Downed Dead Wood Using Terrestrial Laser Scanning." *ISPRS Journal of Photogrammetry and Remote Sensing* 151: 76–90. doi:10.1016/j.isprsjprs.2019.03.007.

Zhang, Y. 2016. "The D-FCM Partitioned D-BSP Tree for Massive Point Cloud Data Access and Rendering." *ISPRS Journal of Photogrammetry and Remote Sensing* 120: 25–36. doi:10.1016/j.isprsjprs.2016.08.002.

Zhang, Z. H., G. L. Chen, X. Wang, and M. C. Shu. 2021. "DDRNet: Fast Point Cloud Registration Network for Large-Scale Scenes." *ISPRS Journal of Photogrammetry and Remote Sensing* 175: 184–198. doi:10.1016/j.isprsjprs.2021.03.003.

Zhang, W. M., J. Shao, and S. N. Jin. 2021. "Automated Marker-Free Registration of Multisource Forest Point Clouds Using a Coarse-To-Global Adjustment Strategy." *Forests* 12 (3): 269. doi:10.3390/f12030269.

Zhang, W. M., P. Wan, and T. J. Wang. 2019. "A Novel Approach for the Detection of Standing Tree Stems from Plot-Level Terrestrial Laser Scanning Data." *Remote Sensing* 11 (2): 211. doi:10.3390/rs11020211.

Zhao, X. Q., Q. H. Guo, Y. J. Su, and B. L. Xue. 2016. "Improved Progressive TIN Densification Filtering Algorithm for Airborne LiDar Data in Forested Areas." *ISPRS Journal of Photogrammetry and Remote Sensing* 117 (3): 79–91. doi:10.1016/j.isprsjprs.2016.03.016.

Zhen, Z., L. Yang, Y. Ma, and Q. B. Wei. 2022. "Upscaling Aboveground Biomass of Larch (*Larix Olgensis Henry*) Plantations from Field to Satellite Measurements: A Comparison of Individual Tree-Based and Area-Based Approaches." *GIScience & Remote Sensing* 59 (1): 722–743. doi:10.1080/15481603.2022.2055381.

Zhou, Y., J. Singh, J. R. Butnor, C. Coetsee, P. B. Boucher, M. F. Case, E. G. Hockridge, A. B. Davies, and A. C. Staver. 2022. "Limited Increases in Savanna Carbon Stocks Over Decades of Fire Suppression." *Nature* 603: 445–449. doi:10.1038/s41586-022-04438-1.

Appendix

Table A1. All the abbreviations used in this study.

Abbreviation	Explanation	Abbreviation	Explanation
ALS	Airborne Laser Scanning	ANOVA	Analysis of Variance
BLS	Backpack Laser Scanning	CAS (Xu et al. 2020)	Coverage Aware Sampling
CSP (Tao et al. 2015)	Comparative Shortest Path	DBH	Diameter at Breast Height
F-OICP	FPFH-based Optimized ICP	FPFH (Rusu et al. 2009)	Fast Point Feature Histogram
GNSS	Global Navigation Satellite System	ICP (Besl and McKay 1992)	Iterative Closest Point
ITCD	Individual Tree Crown Delineation	KD-tree	K-Dimensional Tree
LiDAR	Light Detection and Ranging	MAE	Mean Absolute Error
MLS	Mobile Laser Scanning	NDT (Magnusson 2009)	Normal Distributions Transform
N-OICP	NDT-based Optimized ICP	PDFs	Probability Density Functions
RANSAC (Raguram et al. 2013)	Random Sample Consensus	RMSE	Root Mean Squared Error
R-OICP	RANSAC-based Optimized ICP	RTK	Real-Time Kinematic
SIFT (Lowe 2004)	Scale-Invariant Feature Transform	SPFH (Rusu et al. 2008)	Simplified Point Feature Histogram
TLS	Terrestrial Laser Scanning	TIN	Triangular Irregular Network
Tukey's HSD	Tukey's Honest Significant Difference	ULS	Unmanned Aerial Vehicle Laser Scanning
3D	Three-Dimensional	4PCS (Aiger et al. 2008)	4-Points Congruent Sets